Identification of clayey, silty and sandy soils from the Var deltaic plateau based on piezocone penetration testing

J.F. SERRATRICE
CETE Méditerranée, LRPC d'Aix en Provence

ABSTRACT

This article describes a natural soil identification method based on data measured using a piezocone (CPTu) and presents an application to soils from France's Var deltaic plateau. This method proceeds in two stages: penetrometer point resistance is first broken down into an isotropic part and a deviatoric part by taking into account water pressure and both the drained and undrained strength measured using the triaxial device on soil samples that had been previously cored *in situ*. This decomposition serves to classify soils by distinguishing clayey and silty fine-grained soils, in which high water pressure develops, from the sandy soils where these pressures are either close to the hydrostatic pressure or else negative. The next stage consists of identifying sensitive sandy soils, which feature limited compactness, low strength and are exposed to the risk of liquefaction, by means of analysing the unit lateral friction and effective cone resistance.

Identification des sols argileux, limoneux et sableux du plateau deltaïque du Var à partir de sondages au piézocône

RÉSUMÉ

L'article décrit une méthode d'identification des sols naturels à partir des données mesurées au piézocône (CPTu) et présente son application aux sols du plateau deltaïque du Var. Cette méthode procède en deux étapes : la résistance de pointe pénétrométrique est d'abord décomposée en une partie isotrope et une partie déviatorique en tenant compte de la pression d'eau et des résistances drainées et non drainées mesurées à l'appareil triaxial sur les sols carottés au préalable sur le site. Cette décomposition permet de classer les sols, en distinguant les sols fins argileux et limoneux, dans lesquels se développent de fortes pressions d'eau, et les sols sableux dans lesquels ces pressions sont proches de la pression hydrostatique ou sont négatives. L'étape suivante identifie les sols sableux sensibles, de faible compacité et peu résistants, exposés au risque de liquéfaction notamment, en analysant le frottement latéral unitaire et la résistance de cône effective.

INTRODUCTION

This article proposes a method for interpreting penetrometer data in an effort to identify fine-grained clayey, silty or sandy soils in their natural state. This method is based on an analogy that can be drawn between the behaviour of these soils in the laboratory on the triaxial device and the penetration of a piezocone into these same materials. The method proceeds according to a two-step approach, beginning with measurements recorded during piezocone sounding on borehole samples, i.e. yielding the cone resistance q_c, unit lateral friction f_s and water pressure u_2. At first, the values of q_c and u_2 are used to identify the ground layers crossed during penetration, for the purpose of obtaining the soil layer profile. The second step entails applying the f_s measurement to determine sensitive soils among the sandy ones, i.e. the loosest soils, which may display a risk in terms of liquefaction

for example. The benefit of our method lies in the direct simultaneous use of all three measurements q_c, f_s and u_2 output by the piezocone. This method differs from those typically implemented to interpret penetrometer data from a piezocone since pressure u_2 is introduced as a priority variable while friction f_s is only input during the second step.

The behaviour of both fine-grained soils and sands in laboratory triaxial tests will be recalled first, in terms of stress paths or strain paths and by distinguishing between drained and undrained types of behaviour. This article will then analyse soil behaviour during piezocone penetration before presenting the analogy between triaxial test and piezocone responses, as this analogy provides the basis of the soil identification method developed herein.

The article will then focus on the soil identification method by relying on the data q_c and u_2 generated by piezocone soundings and the triaxial tests performed during the various geotechnical survey campaigns at the Nice Airport site. Afterwards, the identification method for sensitive sands will be explained by comparing piezocone measurements in a layer of silty sands investigated first in its natural state and then after treatment using ballasted columns. The application of this identification method will be illustrated by an analysis of penetrometer data from one of the piezocone soundings tested in 2007 at the *Nice-Côte d'Azur* Airport site.

SOIL BEHAVIOUR MEASURED WITH THE TRIAXIAL DEVICE

All analyses of soil behaviour determined using the triaxial device assume that the total and effective stresses and water pressures are homogeneous throughout the specimen. In reality, this homogeneity can only be approximated, which introduces a level of uncertainty into the test conclusions. We have nonetheless retained this hypothesis in the following analyses.

Failure criterion and stress paths

In the (p',q) reference coordinate system, where the stress deviator q is represented as a function of the average effective stress p', the Mohr-Coulomb criterion:

$$\tau = c' + \sigma' \tan\varphi'$$

can be expressed in the following form:

$q = C'_{qc} + M_c p' = \dfrac{6\cos\varphi'}{3-\sin\varphi'} c' + \dfrac{6\sin\varphi'}{3-\sin\varphi'} p'$ in the compression tests (i.e. where the effective vertical stress σ'_a exceeds the effective radial stress σ'_r)

and:

$q = C'_{qe} + M_e p' = -\dfrac{6\cos\varphi'}{3+\sin\varphi'} c' - \dfrac{6\sin\varphi'}{3+\sin\varphi'} p'$ in the tensile tests (where $\sigma'_a < \sigma'_r$).

The conventional soil strength parameters c' and φ' are correlated with the coefficients of the boundary lines in the (p', q) coordinate system via the following relations:

$$\sin\varphi' = \frac{3M_c}{6+M_c} = -\frac{3M_e}{6-M_e},$$

$$c' = \frac{C'_{qc}\left(3-\sin\varphi'\right)}{6\cos\varphi'} = -\frac{C'_{qe}\left(3+\sin\varphi'\right)}{6\cos\varphi'}.$$

Analogous expressions apply under consolidated undrained conditions (i.e. triaxial tests CU+u), with the corresponding notations containing the index u: C_{qcu}, C_{qeu}, M_{cu}, M_{eu}, c_{cu} and φ_{cu}.

Pore pressure at failure during consolidated undrained testing

When the soil fails in compression, the effective stresses verify the equation:

$$q = C'_{qc} + M_c p'.$$

During a CU+u test, the specimen is first subjected to a pore pressure u_{cp} along with an equal isotropic confinement pressure $p_{conf} = u_{cp}$. The next step consists of consolidating the soil under an isotropic pressure p_c and then increasing the axial stress σ_a, which results in creating a stress deviator $q = \Delta\sigma_a$. At the time of failure, the total and effective stresses equal respectively:

$$p_{rupt} = p_{conf} + p_c + \Delta\sigma_a / 3 = p_{conf} + p_c + q_{rupt} / 3$$

$$q_{rupt} = \Delta\sigma_a / 3$$

$$p'_{rupt} = p_{conf} + p_c + q_{rupt} / 3 - u_{cp} - u_{rupt} = p_c + q_{rupt} / 3 - u_{rupt}$$

$$q'_{rupt} = q_{rupt}$$

The pore pressure at failure (on the Mohr-Coulomb line) is thus equal to:

$$u_{rupt} = p_c + q_{rupt} / 3 - p'_{rupt}.$$

Introducing the Mohr-Coulomb criterion expression and eliminating p'_{rupt} then yields:

$$u_{rupt} = p_c + q_{rupt} / 3 - p'_{rupt} = p_c + q_{rupt} / 3 - q / M_c - C'_{qc} / M_c.$$

Between two failure states in compression on the Mohr-Coulomb line, the variation Δu in pore pressure is correlated with the variation Δq in the deviator by means of the relation:

$$\frac{\Delta u}{\Delta q} = -\frac{3 - M_c}{3M_c} = -\frac{1 - \sin\varphi'}{2\sin\varphi'}$$

Between two failure states in tension, the following is similarly obtained:

$$\frac{\Delta u}{\Delta q} = -\frac{3 - M_e}{3M_e} = \frac{1 + \sin\varphi'}{2\sin\varphi'}.$$

These two relations provide expressions for the Mohr-Coulomb criterion in the (q, u) plane in both compression and tension; they may be used to assess the quality of the consolidated undrained triaxial tests (CU+u). It can moreover be observed that:

$$\frac{C_{qc}}{M_c} = \frac{C_{qe}}{M_e} = c\cot\varphi'.$$

Stress paths in undrained tests

› Pattern of the undrained stress paths in clays

Figure 1 presents a schematic view of stress paths (p, q) and (q, u) during triaxial test CU+u conducted on a (slightly) overconsolidated clay; the specimen had been consolidated under an isotropic effective stress p_c of less than the preconsolidation pressure and then loaded in compression at constant confinement pressure ($\Delta q = \Delta\sigma_a - \Delta\sigma_r > 0$; $\Delta\sigma_r = 0$). This pattern holds true for anisotropic consolidation as of a point (p_c, q_c) located inside the pseudo-elastic domain of the soil, with $q_c \neq 0$, or for a tensile loading ($\sigma_a < \sigma_r$; $\Delta q = -\Delta\sigma_r < 0$). The total stress path is represented by a straight line segment of slope 3 in the (p, q) plane, beginning at point (p_c, 0). The failure envelope (Mohr-Coulomb criterion) is a line of slope M_c and *y*-axis intercept C_{qc}.

Four successive parts can be distinguished within the stress path:

– Part 1: Onset of undrained shear. For an isotropic soil, the stress path is vertical ($\Delta p' = 0$; $\Delta u = \Delta p$);

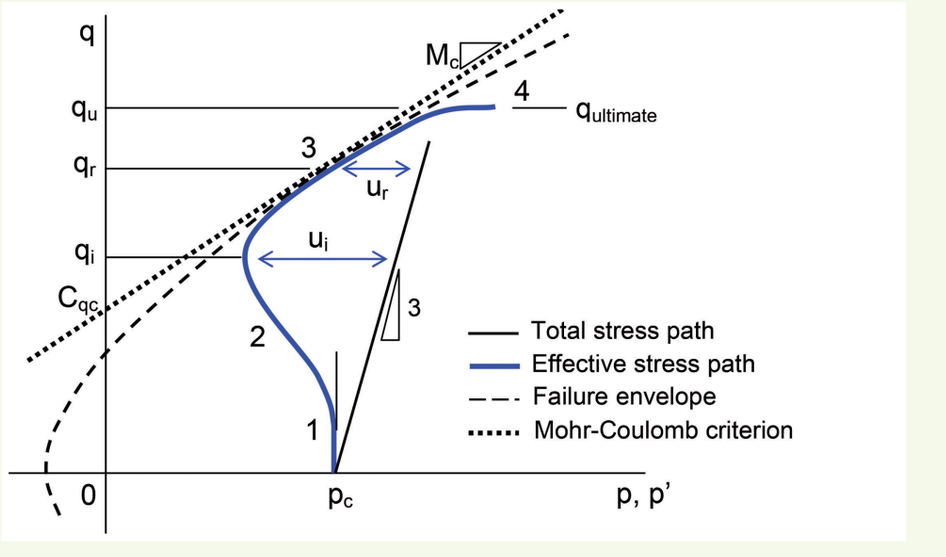

Figure 1
Total and effective stress paths in a consolidated undrained compression triaxial test. Characteristic slopes: 1 - elastic phase; 2 - strain hardening; 3 - failure; and 4 - ultimate strength

– Part 2: Nonlinear contracting behaviour. Compression of the skeleton is accompanied by an increase in pore pressure. Nonlinear and irreversible strains appear, and this part is confirmed when proceeding with cyclic loadings. The water pressure rise depends on: soil saturation, water compressibility, and particle compressibility. For the represented cohesive soil (i.e. featuring a nonzero cohesion), this part of the curve ends by crossing a dilatancy threshold at the beginning of the pore pressure drop;
– Part 3: Failure. The stress path lies along the failure envelope in the direction of increasing average pressures. The soil is dilatant. Pore pressure is decreasing. The stress ratio $\eta = q/p$ is maximized, as is the ratio $K = \sigma'_r/\sigma'_a$ and:

$$\eta = \frac{\Delta q}{\Delta p} = M_c$$

The specimen still features a cylindrical shape at this stage; strains are small and homogeneous;

Part 4: Ultimate state. The ultimate strength is reached with a low-level strain for stiff materials or a plasticity threshold and large strains for soft soils. The soil volume changes only minimally or not at all, while stresses p and q remain constant for an indefinite increase in deviatoric strain. Pore pressure no longer varies. This state can only be reached under special test conditions, by introducing large homogeneous strains. Continuing the test into Phase 3 actually depends on many of the factors listed above, to an even greater extent than during Phases 1 and 2. The loss of strain homogeneity often interrupts the continued loading.

This stress path is also depicted in the (q, u) plane in **Figure 2**. At the beginning of loading (Part 1), $\Delta u/\Delta q = 1/3$. During the third test phase, this ratio equals: $\Delta u/\Delta q = -(3 - M_c) / 3M_c$ in compression and $\Delta u / \Delta q = -(3 - M_e) / 3M_e$ in tension. As stated above, the layout of the undrained path depends, among other parameters, on: soil saturation, water compressibility, and soil particle compressibility.

› Pattern of the undrained stress paths in sands

Figure 3 shows two undrained stress paths derived on sand specimens in a loose state and in a dense state, respectively. Part 2 of the curve exhibits a unique shape for loose sand, with a strength pseudo-peak. In both cases, the third part of the undrained paths follows the failure envelope in the direction of increasing average pressures with dilatancy.

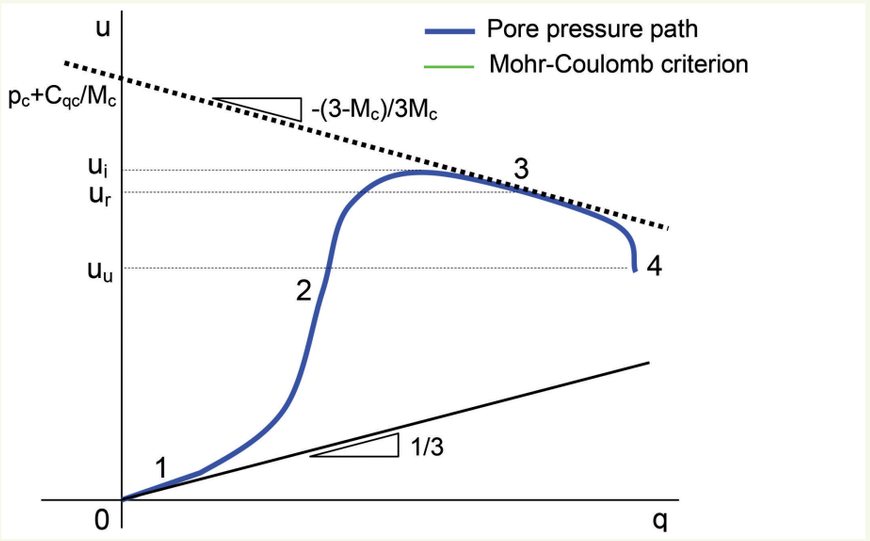

Figure 2
Evolution in the deviator q and pore pressure u during a consolidated undrained compression triaxial test. Characteristic slopes: 1 - elastic phase; 2 - strain hardening; 3 - failure; and 4 - ultimate strength

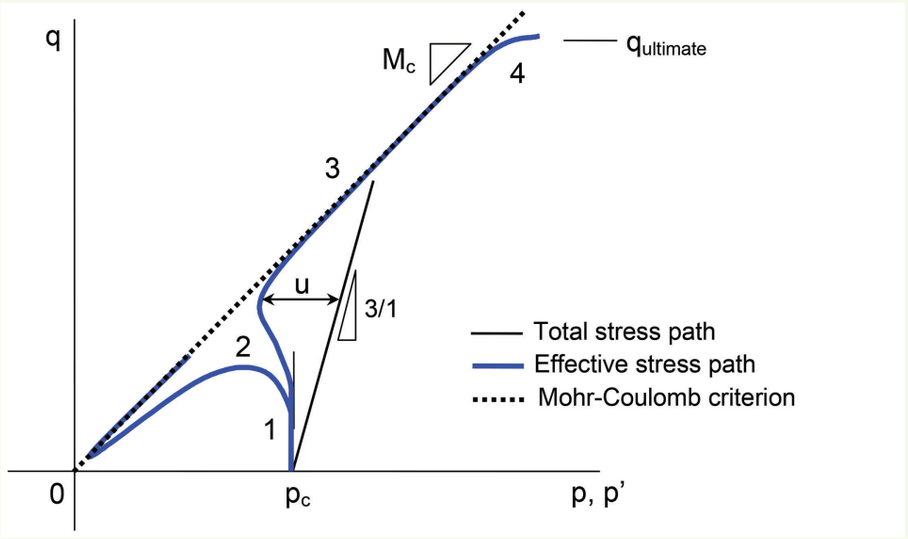

a

b

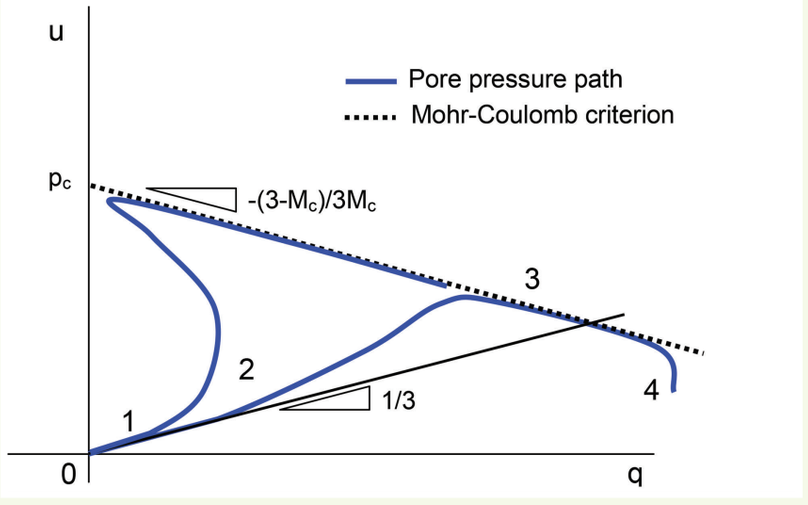

Figure 3
Behaviour of a loose sand specimen and a dense sand specimen during a consolidated undrained compression triaxial test a) in the "average stress p - stress deviator q" plane b) In the "deviator q - pore pressure u" plane

› Remarks regarding the ultimate strength measured with the triaxial test device

The ultimate strength of soft soils is reached in triaxial tests for axial strains typically in excess of 20%. At this point, the specimens are highly deformed, most often in a barrel shape. The strength measurements are dispersed, due in particular to both the influence of soil heterogeneities at the specimen scale and the loss of control over stress and strain field homogeneity in the soil as well as at interfaces with the triaxial heads. This condition is especially true in UU triaxial tests (i.e. unconsolidated undrained specimens). This dispersion sharply increases with material stiffness and cracking, and this trend is more pronounced in rocks, where it is common to observe coefficients of variation on uniaxial compressive strength above 50%, or even more.

Consequently, the straight line determination of ultimate strength is interfered by an additional degree of uncertainty that remains difficult to quantify; to ensure comparability however, the large strains developed around the cone during penetration would require extending the triaxial tests to even higher strain levels.

Undrained stress path shape parameters

In a homogeneous and cohesionless medium (normally consolidated clays and sands), two types of opposite behaviour are apparent:

– Plastic clays reach failure at a stationary point on the Mohr-Coulomb criterion (end of the circular path) $p_r = q_r/M_c$, $q_r = q_{ultimate}$; pore pressure is maximized $u_r = u_{max}$ and the ratio q_r/p_r is also maximized. Steps 3 and 4 overlap **(Fig. 4)**;

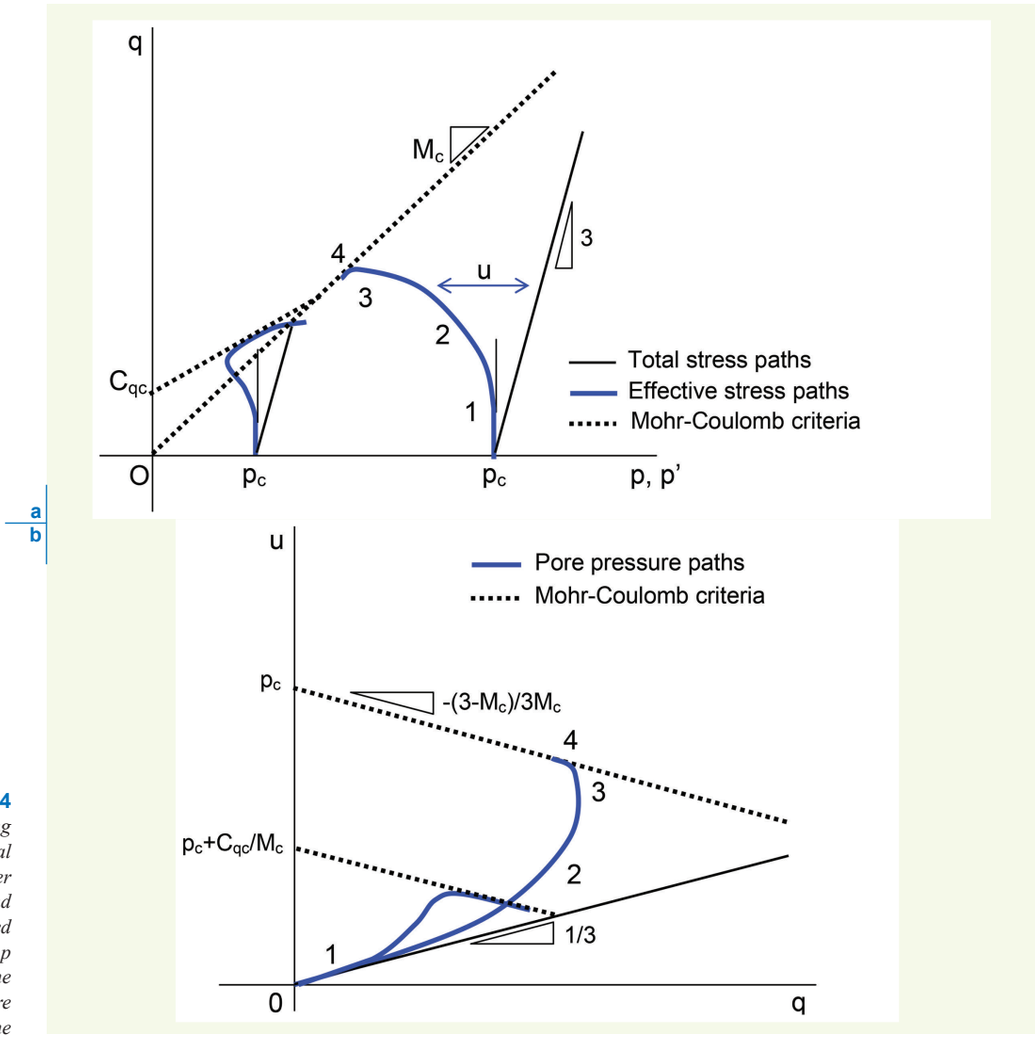

Figure 4
Behaviour of a clay during two compression triaxial tests: consolidated under various pressures and undrained
a) In the "average stress p - stress deviator q" plane
b) In the "deviator q - pore pressure u" plane

– In contrast, the undrained stress paths of sands proceed along the Mohr-Coulomb line, and various specific points may be detected along each curve **(Fig. 2)**:

– the point of maximum pore pressure (p_i, q_i, $u_i = u_{max}$), transition between Parts 2 and 3 of the curve;

– point (p_r, q_r, u_r), where the ratio q/p is maximized, failure point of effective stresses and the "middle" of Part 3 on the curve;

– ultimate strength (p_u, q_u, u_u) occurring in Step 4.

Two indices may now be defined in order to first quantify the shape of undrained paths during Steps 3 and 4 and then provide a depiction of the relationship between q_r and $q_{ultimate}$. These two indices are:

– the ratio between maximum pore pressure and effective consolidation pressure (eventually corrected in the case of anisotropic consolidation):

$$1 - u_i / p_c;$$

– the relative difference between deviators q_i and q_u:

$$(q_u - q_i) / q_i.$$

The deviator q_r lies between q_i and q_u. It will be assumed in the following discussion that $q_r = (q_i + q_u) / 2$.

These two ratios may be standardized by taking into account the slope M_c of the failure criterion, expressed in q/p. For this step, it is proposed to adopt the following normalized slenderness coefficients:

$$R_{ui} = \frac{3(1+M_c)}{3-M_c}\left(1-\frac{u_i}{p_c}\right),$$

$$R_{qu} = \frac{q_u - q_i}{M_c q_i}.$$

The coefficient [3 (1 + M_c) / (3 – M_c)] has been drawn from the expression of an undrained path forming a quarter of a circle in the (p, q) plane (i.e. normally consolidated clay).

The ratio R_{qu} sets the relative position of ultimate strength with respect to the dilatancy threshold. This coefficient equals zero for normally consolidated clays and is very high for sands; it exhibits intermediate values for silts (a behaviour lying between clays and sands) and overconsolidated clays or marls (overconsolidation effect).

The coefficient R_{ui} is correlated with the degree of soil overconsolidation R_{oc}. As such, it may be considered as a strain hardening parameter. In fact, the more a soil is overconsolidated, indurated or dense, the lower the pore pressure peak relative to pressure p_c. On the other hand, soft soils and loose soils generate strong pore pressures compared to p_c, for degrees of overconsolidation near one.

Consequently, the pairs (R_{ui}, R_{qu}) serve to evaluate the slenderness of undrained stress paths, as an indicator of a rise in the failure envelope until reaching either ultimate strength q_u (for sands) or, alternatively, a stationary failure point level (for clays).

Slenderness coefficient values for undrained paths using the triaxial device

We have analysed over 200 triaxial tests of the consolidated undrained type (CU+u) on clays, silts, sands and marls. On each of the drained paths, the characteristic points (p_i, q_i, u_i), (p_r, q_r, u_r) and (p_u, q_u, u_u) were all identified, then the slenderness coefficients R_{ui} and R_{qu} were calculated. The slope M_c was assumed equal to the ratio $M_c = q_r / p_r$. A set of graphs displaying R_{qu} as a function

of R_{ui} were established for each type of material. It would appear that the pairs (R_{ui}, R_{qu}) may be assigned to sectors delimited by curves whose equations are given in **Table 1**. The sectors specific to sands, silts and clays have been shown in **Figure 5**.

Accordingly, the slenderness coefficients deduced from consolidated undrained (CU+u) triaxial tests allow clearly distinguishing the behaviour of slightly overconsolidated clays (stationary stress state at failure, zero R_{qu} value) from the behaviour of sands (rise in the failure envelope, high R_{qu} value), as well as drawing a correlation between the ultimate strength measured on the triaxial device and the dilatancy threshold of the material, which in most cases is simple to identify. The coefficients R_{ui} and R_{qu} enable ranking the various soils into five families on the basis of the undrained stress path shape.

These sectors however are not disconnected. Sandy silts occupy a strip located between silts and sands. On the whole, the R_{ui} coefficients increase with R_{qu}, ranging from soft clays to dense sands. Marls appear within the continuity of the clays, with higher R_{ui} and R_{qu} coefficients; these trends stem from the overconsolidation effect. Here once again, the transition between clays and marls is not clearly defined but rather gradual.

At many sites formed by recent and relatively unconsolidated soil, the soils extracted from the same formation, or even the same layer, are classified into several types of behaviour. These soils are in

Table 1
Limits between soil families according to slenderness coefficients

Material	Lower limit	Upper limit
Sands	$R_{qu} = 0{,}15 \exp(3\ R_{ui} / 5)$	$R_{qu} = 0{,}50 \exp(3\ R_{ui} / 5)$
Silts	$R_{qu} = 0$	$R_{qu} = 0{,}22 \exp(3\ R_{ui} / 5)$
Clays	$R_{qu} = 0$	$R_{qu} = 0{,}03 \exp(3\ R_{ui} / 5)$
Plastic clays	$R_{qu} = 0$	$R_{qu} = 0{,}012 \exp(3\ R_{ui} / 5)$
Marls	$R_{qu} = 0$	$R_{qu} = 0{,}16 \exp(3\ R_{ui} / 5)$
Fissured marls	$R_{qu} = 0$	$R_{qu} = 0{,}01 \exp(3\ R_{ui} / 5)$

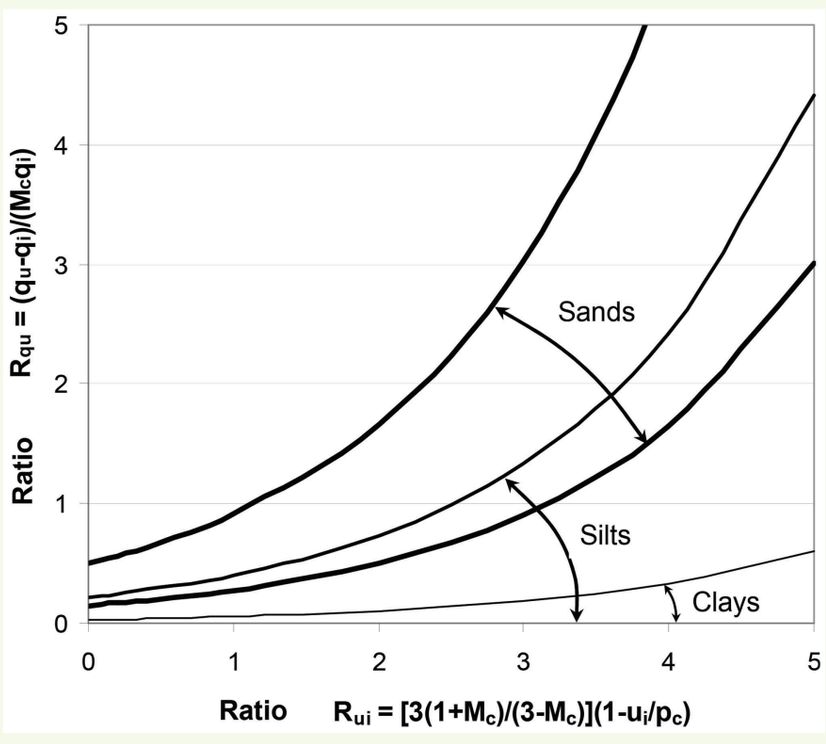

Figure 5
Identification of soil types as a function of the slenderness coefficient values of stress paths found in consolidated undrained compression triaxial tests

fact heterogeneous and composed of clays, silts, loams and sands, with responses (R_{ui}, R_{qu}) that span the entire spectrum from clays to sands. These Quaternary materials are often deposited in beds of various thicknesses and interlocked within soil layers, with a vertical variability of their mechanical properties on the order of 10 cm, equivalent to the scale of triaxial specimens.

SOIL BEHAVIOUR DURING PENETRATION OF A PIEZOCONE

Piezocone measurements

The piezocone tests (CPTu) serve to measure tip resistance q_c, unit lateral friction f_s and water pressure u_2, which is most frequently measured immediately in back of the cone during penetration at constant speed (2 cm/s). These measurements are not completely independent. The stress, pore pressure and strain are not homogeneous around the penetrometer tip; moreover, interaction occurs between the soil and the tip.

Nonetheless, the test makes it possible to clearly distinguish the response of dense sandy soils from that of soft clayey soils:

– in saturated soft clays, penetration generates strong water pressures u_2 that increase with depth. The strengths q_c and f_s also rise with depth. The soil behaviour is undrained. Tip resistance is lower due to the weaker soil shear strength under these conditions and to the low average effective pressures developing in the soil;
– in sands that are clean, dense and saturated, the high ground permeability suppresses all pore pressure build-up and the soil behaviour around the tip is drained. Pressure u_2 remains equal to the hydrostatic pressure u_o. The high strengths typically observed in dense sands originate from the interaction between the tip and the ground, which is stiff and dilatant. In such materials, the variations in q_c and f_s, often recorded along the penetrometer profile, stem from the variability in both the type and state of the sand specimen at a local scale.

Around the tip, a large strain regime arises since the expanded diameter extends from zero in front of the tip to the cone diameter in back, thus inducing tremendous shear. In the immediate vicinity of the cone and as long as no rejection is encountered, the soil is mobilized at its ultimate strength, which is obtained under drained conditions for clean sands and under undrained conditions for clays. These drainage conditions depend on the ratio of soil permeability to penetration speed.

From a mechanical standpoint, the soil loading via the penetrometer tip is of a highly isotropic type, with the deviatoric component being of lesser magnitude. Efforts to model penetration on the basis of expanding spherical or cylindrical cavities were, for this very reason, quite successful.

Theoretical studies and physical models

Many studies have been devoted to the cone penetration problem in soils under confined conditions (over their depth). The most relevant breakthroughs were obtained by reliance on the theory of expanded cavities, whether cylindrical or spherical, applied to punching. The approach using physical models consists of conducting penetrometer tests inside the calibration chambers. Only a very succinct overview of these results is provided herein, by highlighting the main set of problem input parameters.

In cohesive media, the various theoretical developments relative to penetration lead to a relationship between the undrained strength c_u of clays and the tip resistance, which can be written in the following form:

$$q_c = N_c\, c_u + \sigma_o$$

where N_c is a theoretical factor and σ_o a total stress representing total stresses in the soil at a given level (vertical stress σ_{vo}, horizontal stress σ_{ho} or average stress σ_{mo}). Various expressions have been proposed for factor N_q, featuring the following parameters:

– σ'_o: an effective stress (vertical, horizontal or average)
– K_o: coefficient of earth pressure at rest
– R_{oc}: degree of overconsolidation
– I_r: soil stiffness index ($I_r = G / c_u$), where G is the soil shear modulus and c_u its undrained cohesion
– φ': effective angle of friction for the soil
– M_c: corresponding slope in the (p', q) triaxial plane
– δ: a term reflecting friction at the cone-soil interface
– v: penetration speed.

The degree of overconsolidation is most often defined in terms of vertical stresses, but average stresses would also be appropriate. The shear modulus G remains constant, yet not necessarily linear at all times, and dependent on both the stress and shear strain levels found in the soil. The presence of the stiffness index in formulations allows introducing the elastic reaction of a soil at the plastic zone boundary that develops around the cone, while cohesion c_u adds to the soil's undrained strength.

These same parameters are involved in the formulations relative to pore pressures generated by penetration into saturated clays. Chang *et al.* (2001) presented a theoretical analysis of piezocone penetration in clays on the basis of the modified Cam-Clay model; they derived the following expressions for c_u, q_t and u_2:

$$c_u = \frac{M_c}{2}\sigma'_{vo}\left(\frac{R_{oc}}{2}\right)^{\Lambda}$$

$$q_t = \frac{4}{3}\alpha_e c_u\left(1+\ln I_r\right)+p_o$$

$$u_2 = 2\alpha_e c_u\left(\frac{1}{\sqrt{3}}\ln\frac{\sqrt{3}I_r}{2}-\frac{1}{M_c}\right)+p_o$$

where α_ε is a factor correlated with the penetration speed ($\alpha_\varepsilon = 1.64$ for a 10-cm^2 cross-section cone), M_c the slope of the Mohr-Coulomb line in the effective stress plane (p, q) in compression, R_{oc} the degree of overconsolidation, I_r the stiffness index, Λ the coefficient of plastic volumetric strain ($\Lambda = 1 - \kappa/\lambda \approx 1 - C_s/C_c$), p_0 the average total stress, and σ'_{v0} the effective vertical stress.

In sands, developments based on the cavity expansion theory refer to the parameters σ'_o, K_o, e, $I_r = G/c_u$, φ' or M_c, ψ and δ. The notations are the same as those provided above, along with e for the soil void index and ψ for dilatancy. The void index is in fact often introduced via the density index I_D:

$$I_D = \frac{e_{\max} - e_{\min}}{e_{\max} - e_{\min}},$$

where e_{max} and e_{min} are the maximum and minimal sand void indices. This parameter is of obvious benefit in representing the state of clean and dry sands reconstituted in the laboratory. Its practical value however is limited by the fact that the index cannot be efficiently determined in saturated natural soils, especially in soils containing fines, due to its inability to replicate sedimentation conditions in water and the evolution of deposits over time (just like the index of consistency, $I_C = (w_L - w) / (w_L - w_P)$, which resembles I_D for unstructured clays).

Some studies have made use of the parameter ξ (correlated with the void index), which denotes the distance between void index e and void index in the critical state e_{CS} with the same average effective pressure p'.

In many instances and by reliance on theoretical developments, the authors have sought to deduce the penetrometer strength q_c, mechanical properties or soil condition, c_u, R_{oc}, φ', ψ, I_D or ξ, by means of an approach opposite the one recommended in the present study, which consists of decoding the penetrometer response based on prior knowledge of soil strength properties measured using the triaxial device.

Another difficulty lies in the absence of developments focusing on unit lateral friction f_s, despite its use as the basis for many soil classification protocols and stability calculation methods, specifically related to liquefaction.

Along these lines, it is important to determine whether the frequently observed increase in penetrometer strength with depth stems from solely the confinement pressure provided by the weight of ground, or the natural increase in strength that the soil has acquired during its sedimentation followed by its evolution over time, or else both of these acting together. The penetrometer measurement standardization methods embedded into the stability calculation methods actually depend on the answer to this question.

Evolution of penetrometer strength with depth

Many penetrometer recordings obtained in soft clays and published in the literature show a quasi-linear increase in measurement results vs. depth. **Table 2** lists a few examples of increasing penetrometer measurement trends relative to depth found in clays.

The increasing gradients of q_c with z vary between 30 and 50 in clays, while those of u_2 range from approx. 25 to 40. For cone resistance q_c, this result is explained by the empirical relation yielding the evolution in undrained cohesion with depth. By combining the average relation between undrained cohesion and effective stress in normally consolidated clays ($c_u = \sigma'_{v0} / 3$) with the average relation between cone resistance and undrained cohesion ($q_c = 15\ c_u$) as well as the relation between vertical effective stress, unit weights of both the soil and water and depth in the case of a surface

Table 2
Examples of increasing piezocone measurement trends (CPTu) vs. depth (clays)

Soil	Authors	$\Delta q_c/Dz$ (kPa/m)	$\Delta f_s/Dz$ (kPa/m)	$\Delta u_2/\Delta z$ (kPa/m)
Bothkennar clay	Nash *et al.* (1992)	43	0.46	32
Marine clay	Schneider *et al.* (2001)			42
Silty clay	De Mio and Giacheti (2007)	34 - 57	1	40
Silty clay		23	1 - 4	25 - 35
Clays and silts (sands)	Simonini and Cola (2000)	70	1	27
Soft silty clay	Cetin *et al.* (2004)	30	0,4	26
Soft silty clay		39	0.6	32
Clay to silty clay		25		31
Clay to silty clay		26	0.3	24
Mud and silts	LRPC - Aix-en-Provence	46		(33)
Mud and silts		27		
Mud and silts		29		(37)
Clayey-sandy silt		32	0.3	26
Clayey-sandy silt		26	0.2	30
Clayey-sandy silt		24	0.2	26
Clayey-sandy silt		18	0.2	26
Clayey-sandy silt		18	0.2	24

water layer [$\sigma'_{v0} = (\gamma - \gamma_w)\, z$], then the relation $q_c = 5\,(\gamma - \gamma_w)\, z$ can be derived. For $\gamma = 18$ kN/m^3 and $\gamma_w = 10$ kN/m^3, this result becomes:

$$q_c = 40\, z \qquad \text{(with } q_c \text{ in kPa and z in m)}$$

The formulation based on the Cam-Clay model yields similar results (Chang *et al.*, 2001). By assuming for example that $M_c = 1.2$ ($\varphi' = 30$ degrees), $R_{oc} = 1$ (normally consolidated clay), $I_r = 100$ (soft soil) and $\Lambda = 0.9$, the relations indicated in Section 2.2 become:

$$c_u = 0.322\, \sigma'_{vo}$$
$$q_t = 12.2\, c_u + p_o$$
$$u_2 = 5.68\, c_u + p_o.$$

Next, by assuming $K_o = 0.5$, p_o can be written as: $p_o = 2\, \sigma'_{vo} / 3 + u_o$. For $\gamma = 18$ kN/m^3 and $\gamma_w = 10$ kN/m^3, the following are obtained:

$c_u = 2.5\, z$ (c_u in kPa and z in m)
$q_t = 47\, z$ (q_t in kPa and z in m)
$u_2 = 30\, z$ (u_2 in kPa and z in m).

These relations provide orders of magnitude for the gradients that agree with observations (e.g. slopes on the diagrams in **Figs. 15** and **18**).

ANALOGY BETWEEN THE TRIAXIAL TEST AND THE PIEZOCONE TEST

The method described herein consists of establishing a direct correspondence between soil behaviour observed in the laboratory by use of triaxial tests and the behaviour of these same soils during piezocone tests. The parallel drawn between triaxial and piezocone tests however is not direct since the stress and strain paths remain unknown around the cone during penetration, in addition to these fields not being homogeneous. Nonetheless, a link can be built between these two loading types, by assuming the soil to be maintained in an ultimate failure state in the immediate vicinity of the cone throughout a penetration in steady-state mode. Knowing both soil strength modes, i.e. in effective stresses and total stresses, may be used advantageously in order to decode the penetrometer response, by considering that the soil strength upon cone penetration can be broken down into an isotropic term, expressed as a total stress p_c, and a deviatoric term q_c. Water pressure u_2 is to be subtracted from the isotropic term for the purpose of defining an equivalent average effective pressure p'_c.

Figures 6 and **7** show the correspondence between measured soil responses in the triaxial and piezocone tests, for both the sand and clay cases, respectively.

SOIL IDENTIFICATION METHOD

The first step of the proposed method consists of classifying the soils based on penetrometer measurements, in comparison with the strength measurements recorded on the triaxial device. The presentation of this method will rely on results from geotechnical survey campaigns of the Nice Airport site, which offers both piezocone soundings and core samples, used in conducting identification tests and triaxial tests.

Strength values measured during triaxial tests

The soils of the Var Delta underlying Nice Airport (*Alpes-Maritimes* department) are composed for the most part of clayey silts and sandy silts, in association with incursions of silty sands in layers tens of centimetres to a metre thick. Sandier beds are also encountered within the silty layers.

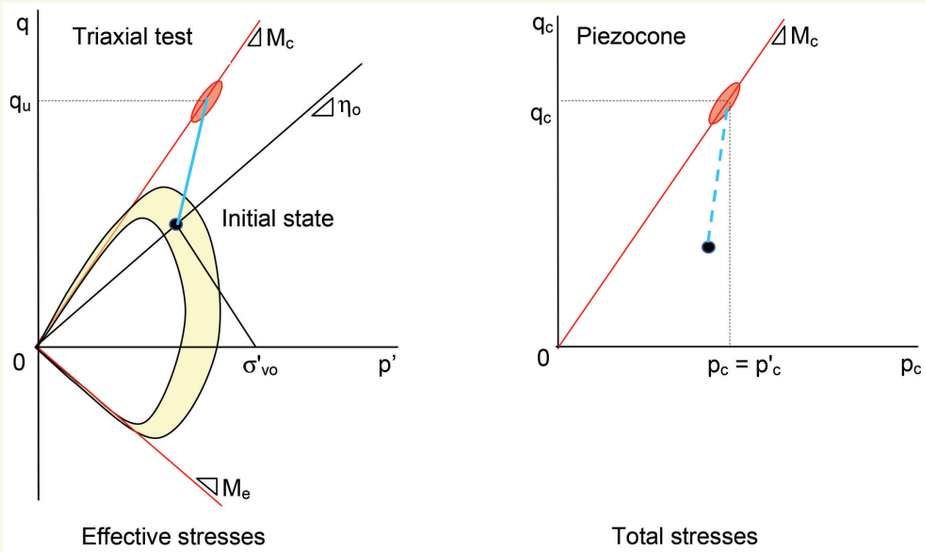

Figure 6
Analogy between a compressive triaxial loading and soil loading by the tip of a piezocone, in the case of a sand specimen

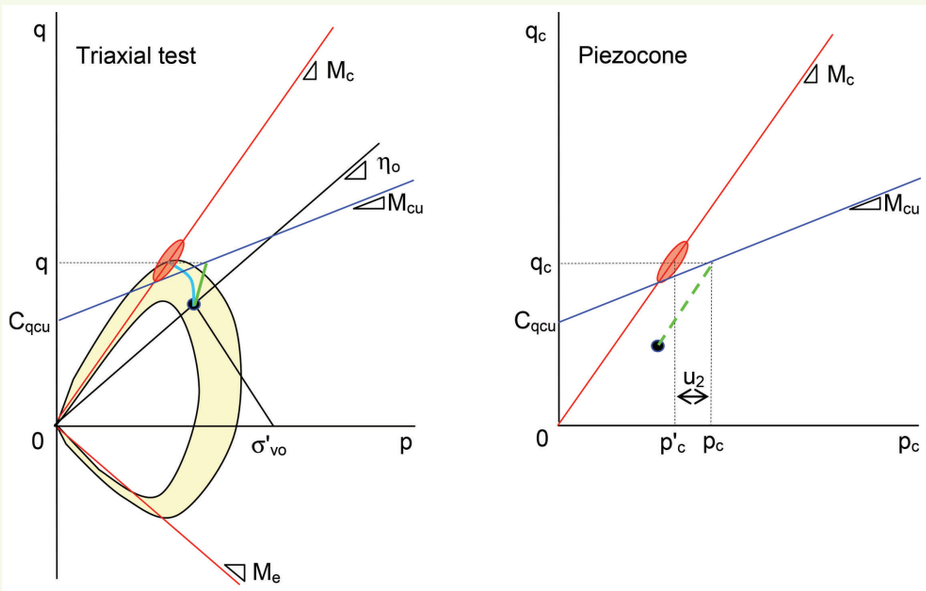

Figure 7
Analogy between a compressive triaxial loading and soil loading by the tip of a piezocone, in the case of a clay specimen

The triaxial tests were conducted on specimens cut in core samples extracted using a stationary piston sampler. These undrained triaxial tests are of the CU+u type and interpreted in effective stresses within the (p', q) plane. They reveal the typical behaviour of granular materials, with angles of internal friction φ' lying between 32.3 and 40.4 degrees. The effective cohesion values are zero or near zero (c' ≈ 0). **Figure 8** compiles the results of these tests, which do not enable differentiating special soil types. Soils with the highest clay content include a high enough silty-sandy fraction to yield a behaviour near that of sands.

The most clayey soils **(Fig. 9)** display an overconsolidated behaviour at very low pressure and are not strictly stationary at high pressure (the undrained stress paths tend to follow the Mohr-Coulomb line upward, with low dilatancy, instead of becoming attached like the soft clays). The silty sands **(Fig. 10)** show a significant rise in stress paths along the Mohr-Coulomb line, with high dilatancy. The sandy silts **(Fig. 11)**, on the other hand, display an intermediate behaviour.

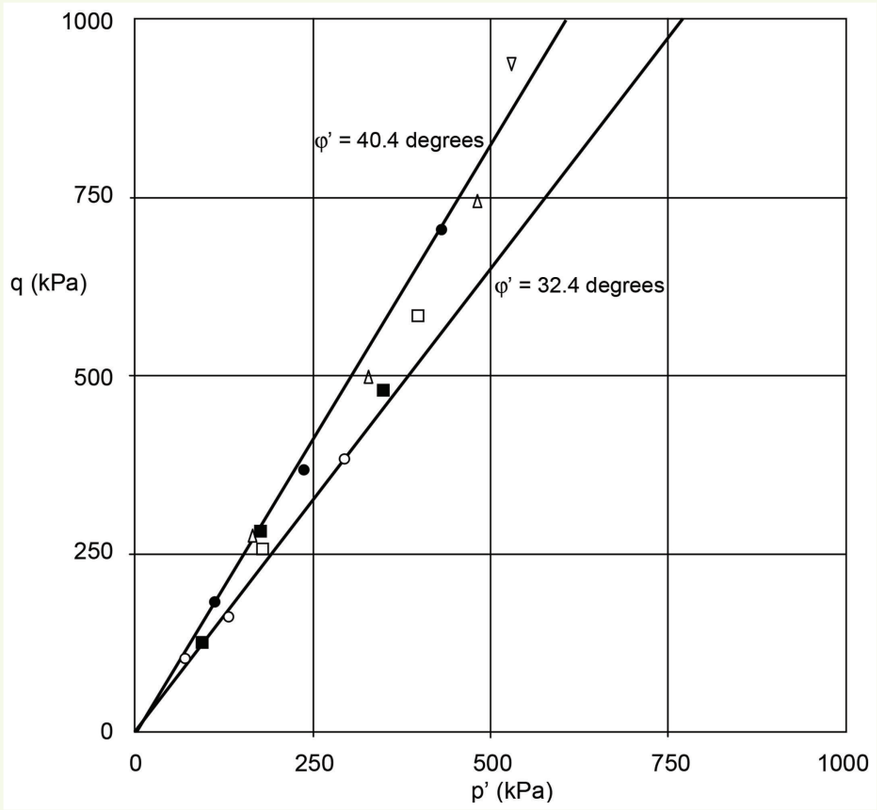

Figure 8
Triaxial compression test results on various in situ soils

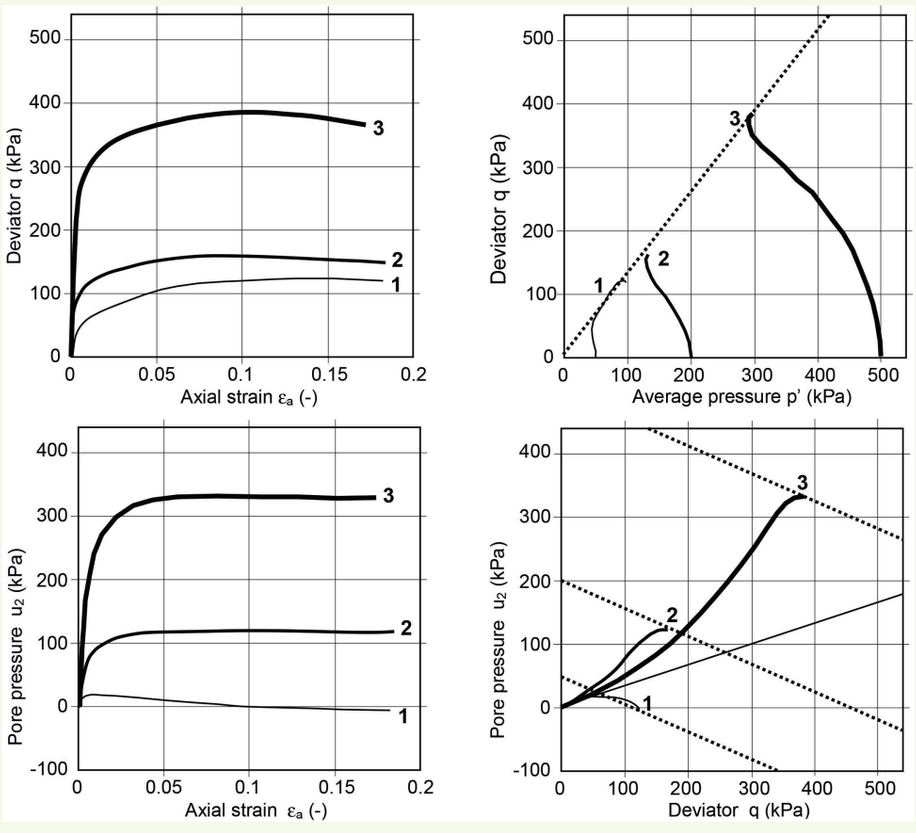

Figure 9
Stress paths for a compression test conducted on a clayey silt specimen

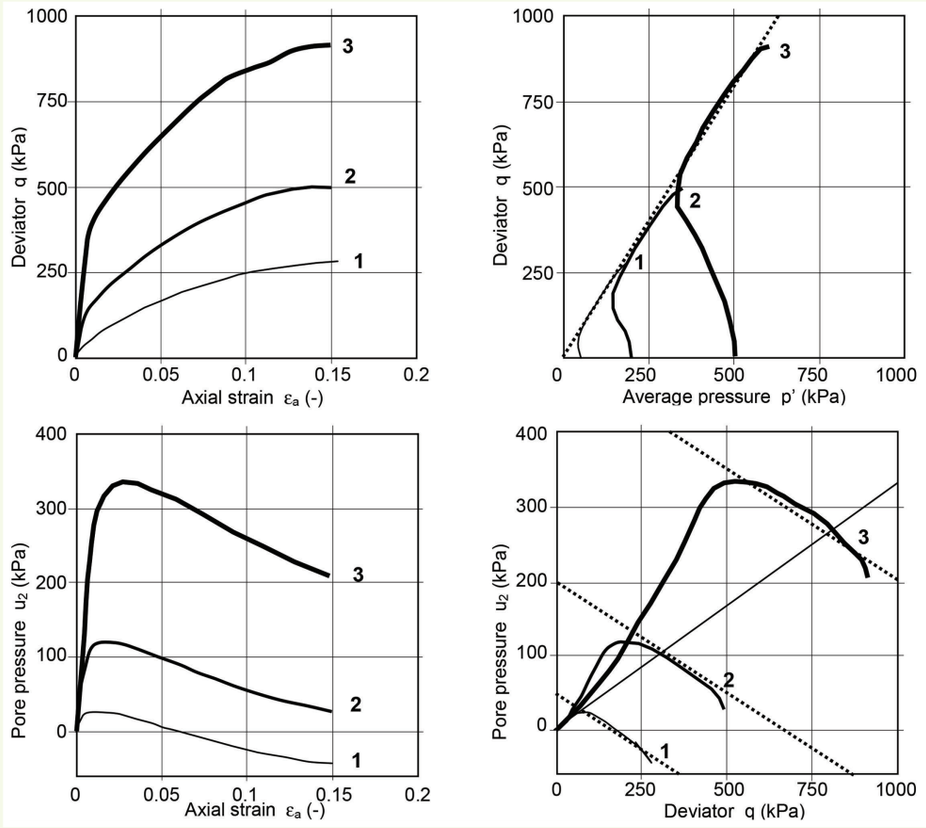

Figure 10
Stress paths from a compression test conducted on a silt specimen

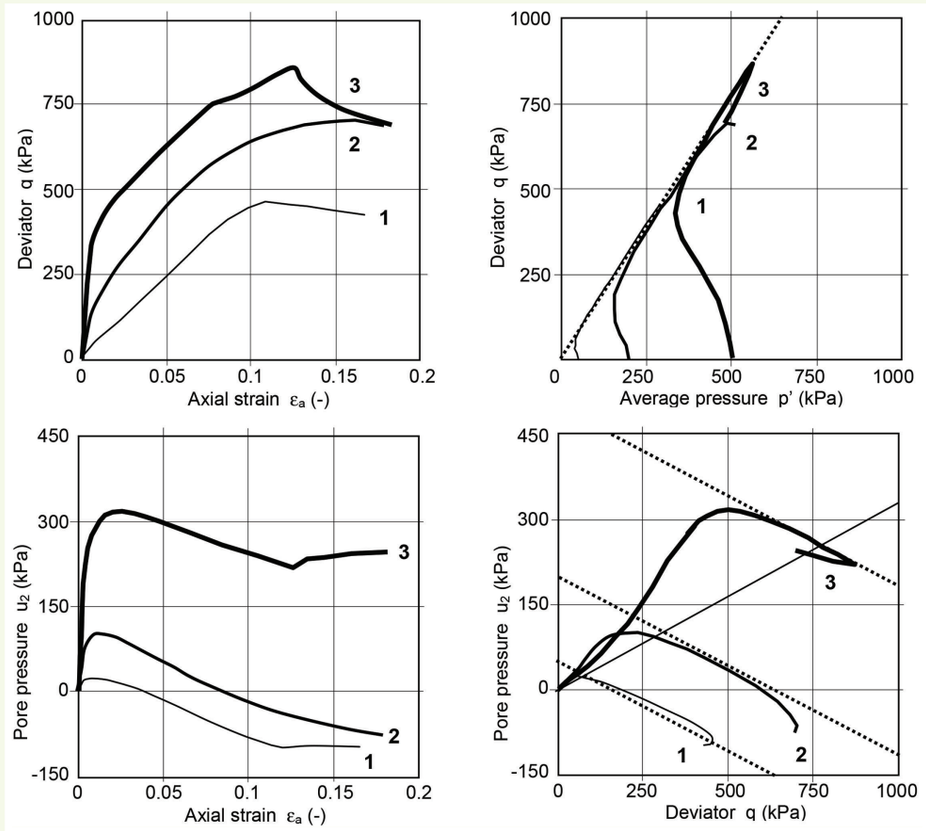

Figure 11
Stress paths for a compression test conducted on a very fine-grained sand specimen

In contrast, the interpretation of total stress tests performed in the (p, q) plane reveal distinct types of behaviour, due to the presence of highly differentiated values of the pore pressure found at failure as well as to the role of dilatancy. **Figure 12** presents the extreme Mohr-Coulomb lines derived from the CU+u triaxial tests interpreted using total stresses. These lines represent the undrained behaviour of both clayey silts and silty sands, respectively. An intermediate line may be selected in order to depict the strength of sandy silts. These three lines encompass the types of behaviour exhibited by the various soils according to these triaxial test results. A fourth line may be defined for dense silty sands, with a very steep slope so as to represent the behaviour indicated by the triangle placed on the top left-hand side of the graph, which corresponds to the strength of a specimen cut out within this type of material. The piezocone however does not serve to detect this type of behaviour, due to the absence of back pressure. **Table 3** summarizes the undrained strength properties determined on the various materials studied herein.

For each soil studied, these mechanical properties characterize the effect of depth on strength (effect of earth weight as a confinement pressure).

Application to the piezocone

We accept that the soil strength values measured with the piezocone in Var sediments are expressed by the lines shown in **Figure 13**, both in the equivalent effective stress plane (p'_e, q_e) and in the equivalent total stress plane (p_e, q_e). The continuous line is drawn using effective stresses

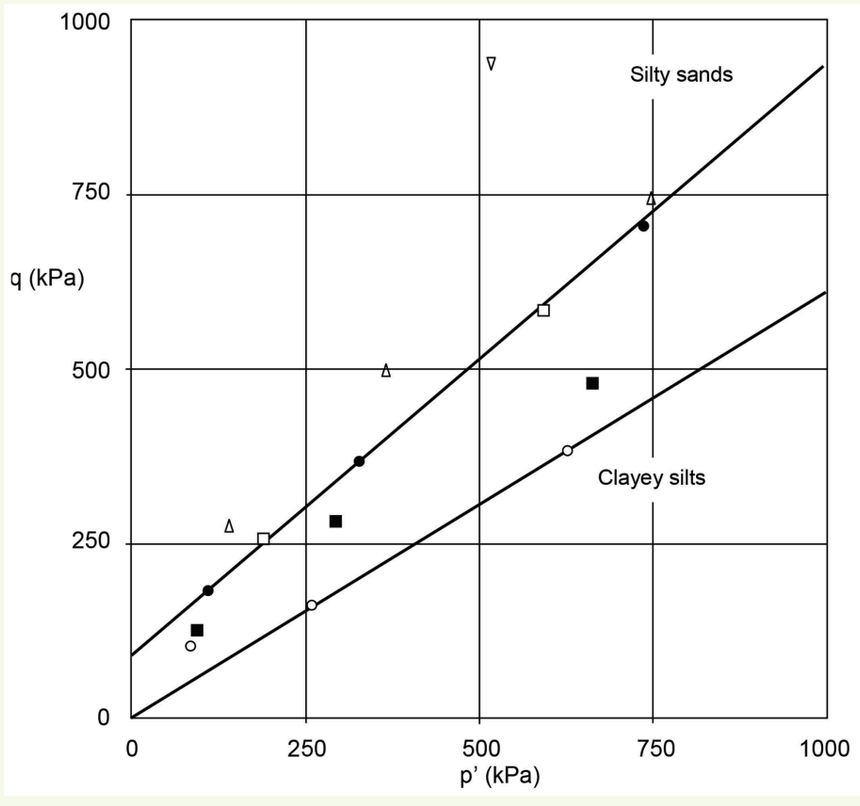

Figure 12
Results of triaxial compression tests conducted on various in situ soils, as interpreted using total stresses

Soil	C_{qcu} (kPa)	M_{cu} (degrés)	c_{cu} (kPa)	φ_{cu} (degrees)
Clayey silts	50	0.70	24	18.3
Sandy silts	100	1.10	48	27.7
Silty sands	200	1.50	100	36.9

Table 3
Undrained strength characteristics of Var Delta soils

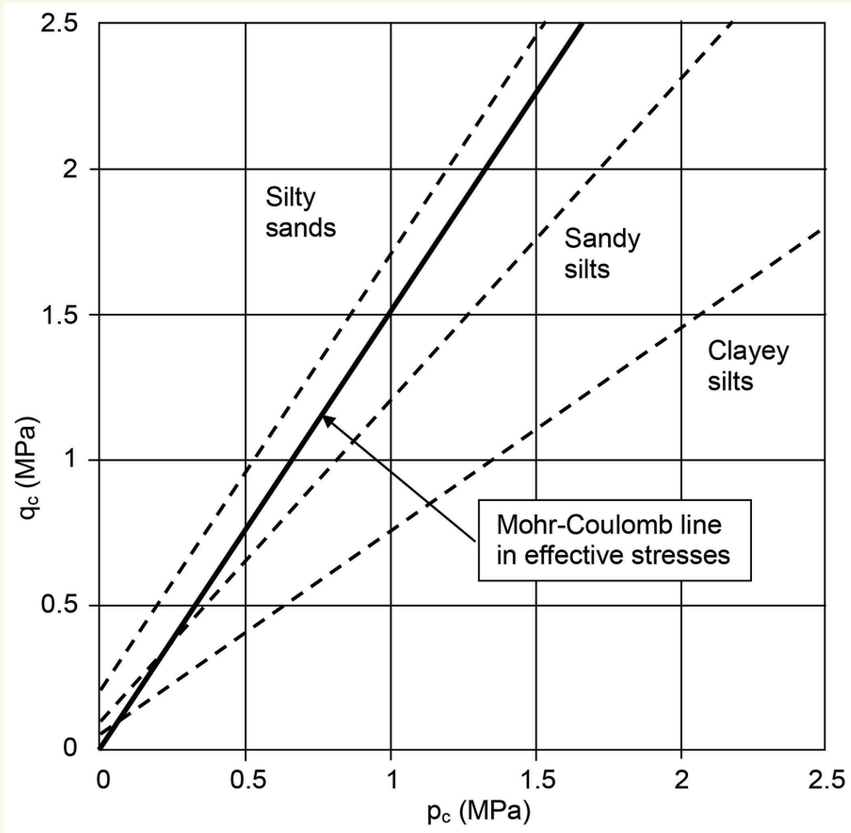

Figure 13
Soil failure criteria in both effective stresses and total stresses

(φ' = 36.9 degrees and c' = 0) and corresponds to the average of Nice soils (M_c = 1.5 and C_{qc} = 0). The three other (dashed) lines represent the "consolidated undrained" strengths expressed in total stresses, corresponding to the values of φ_{cu} and c_{cu} listed in **Table 3**; these lines are assigned respectively to "clayey silts", "sandy silts" and "silty sands".

The following hypotheses are adopted:

– the penetrometer thrusts the soil into its ultimate state on the Mohr-Coulomb line defined in effective stresses;
– the cone resistance q_c of the piezocone is equal to the deviator q of the triaxial test;
– the tip generates an equivalent average total pressure p_c, which depends directly on q_c and u_2;
– the pressure u_2 measurement is representative of "total pore pressure" in the tip vicinity, except in the case of cavitation for undrained dense sands.

In the (p_c, q_c) graph, the measured q_c value serves to determine the "equivalent average effective stress p'_c generated by the tip" on the "effective" line. The "equivalent average total stress" p_c is obtained by adding to p'_c the measured value of u_2, which yields the coordinates (p_c, q_c) of the point representing the equivalent total stress state around the cone. The three lines defined in "total stresses" to represent soil strength are then considered, and the one located closest to this point is chosen to classify the soil. **Figure 14** shows an application of this procedure to q_c and u_2 measurements at three depths lying between 19.22 m and 19.64 m in the CPTu12 borehole drilled at the airport site. The corresponding soils were classified as: silty sand, sandy silt, and clayey silt.

Once the identification step has been performed for all measurements collected in a borehole, results can be displayed on the standard depth variation diagrams of: cone resistance q_c, unit lateral friction f_s, and measured water pressure u_2. **Figure 15** shows the soil ranking from the CPTu20 borehole. The measurement points are coded as: silty sands (SL), sandy silts (LS) and clayey silts (LA). It clearly appears that the strongest pressures u_2 are ascribed to clayey silts, with the weakest

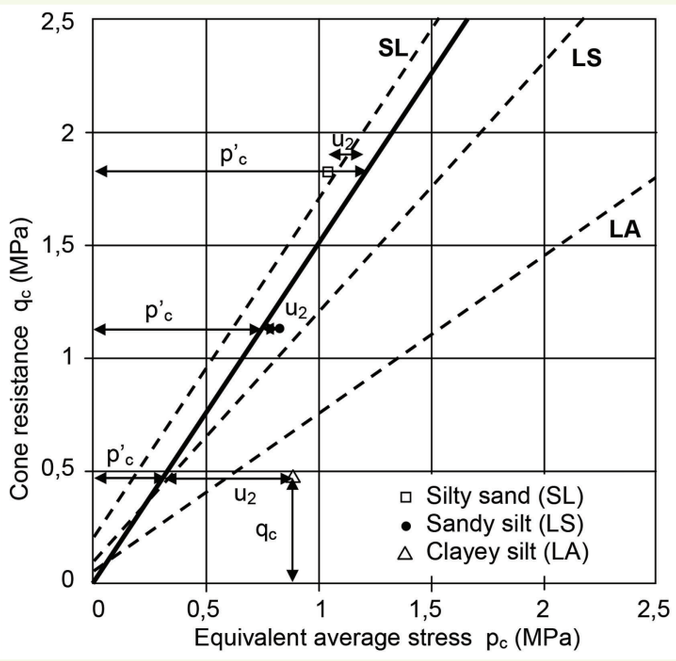

Figure 14
Application of the soil identification method at three depths in a borehole

pressures attributed to silty sands. **Figure 16** shows a close-up of **Figure 15** for depths between 10 and 25 m (relative to the embankment surface).

Figure 15
Representation of the various soil types (clayey silts: LA, sandy silts: LS, and silty sands: SL) vs. depth (for borehole CPTu20)

The soil classification process may also be reported on the (p_c, q_c) diagrams. **Figure 17** conveys the results from borehole CPTu20 according to this same mode of representation. **Figure 18** then provides an enlargement of the diagram in **Figure 17** for the weakest soils (i.e. strength between 0 and 3 MPa).

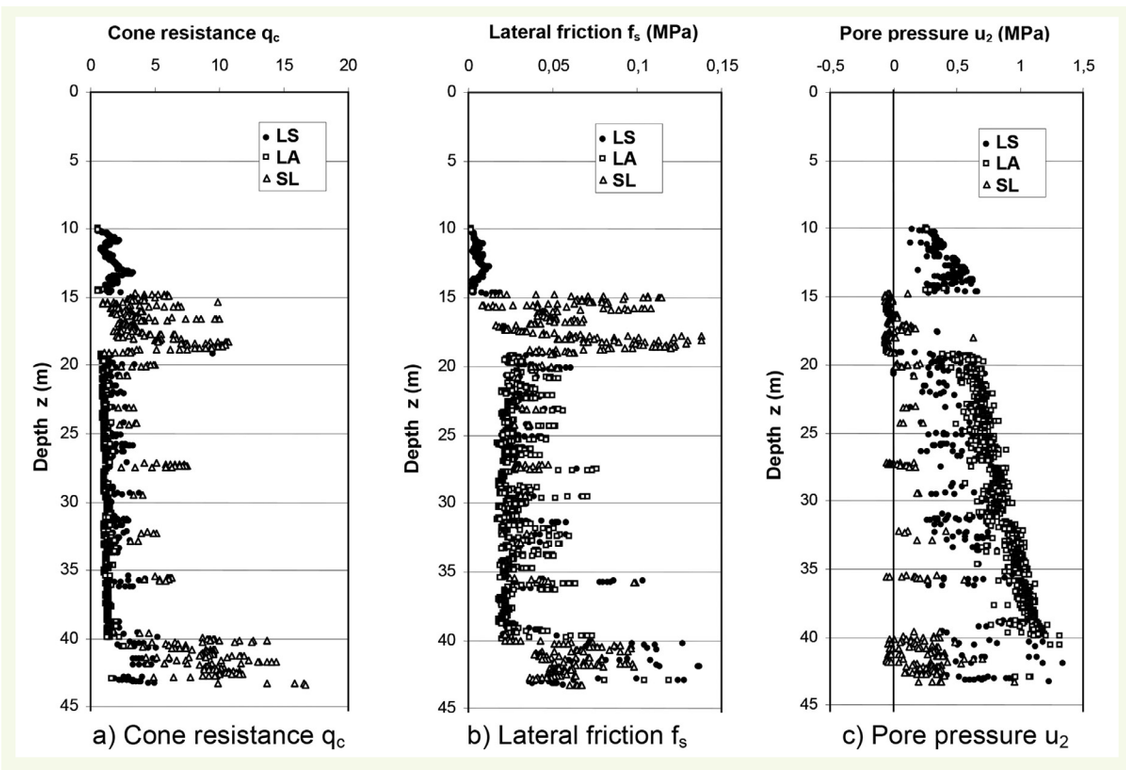

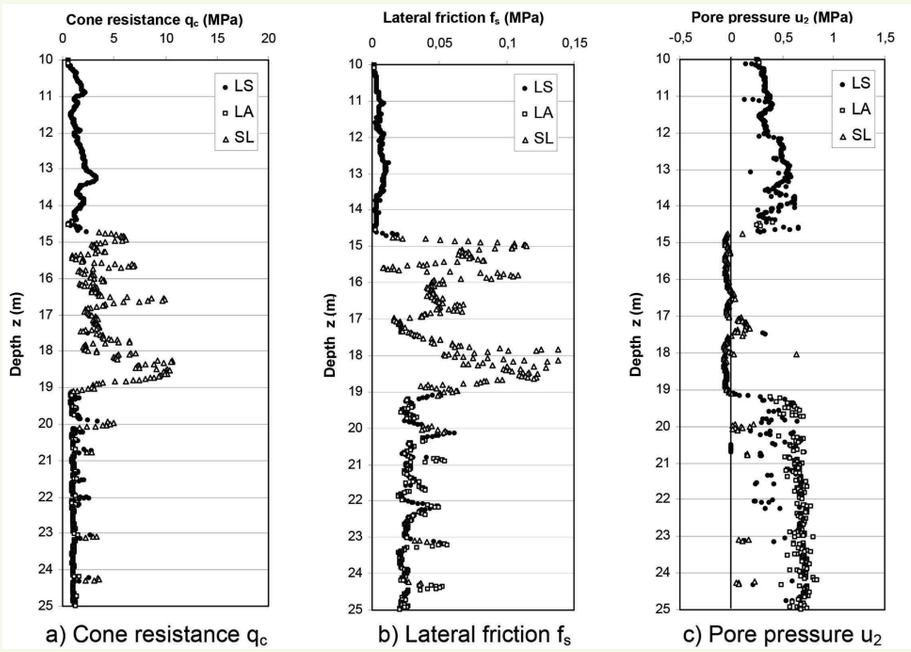

Figure 16
Close-up of Figure 15

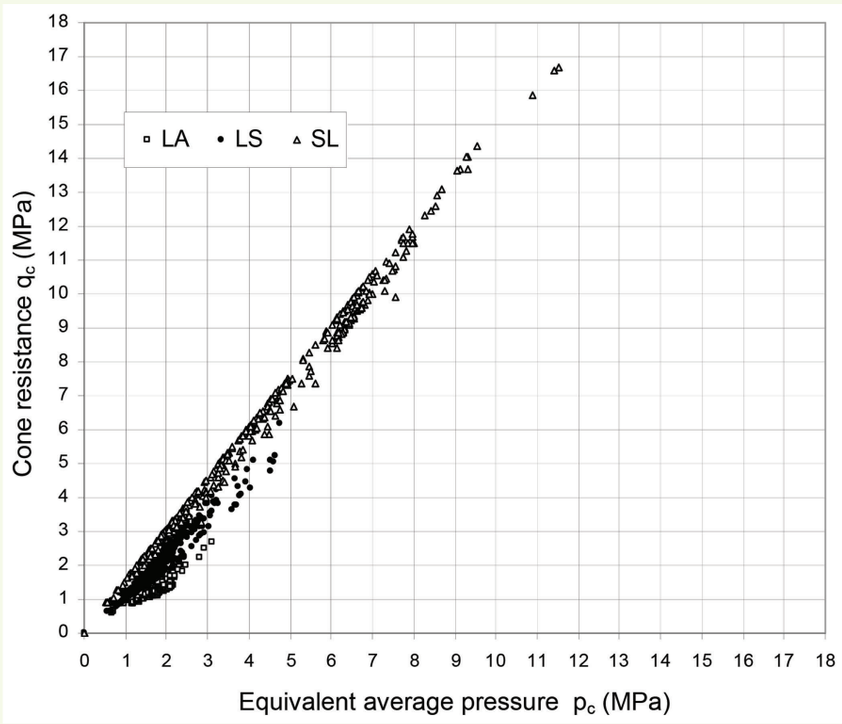

Figure 17
Representation of the various soil types (clayey silts: LA, sandy silts: LS, and silty sands: SL) in the (p_e, q_c) diagram (CPTu20 borehole)

Comments

› Problems associated with the u_2 measurement

The water pressure u_2 measurement using the piezocone meets some experimental difficulties along this interface, which slides into the destructured soil in back of the cone: this interface may constitute a preferential drainage path or promotes the formation of a water column between the push rod and the soil.

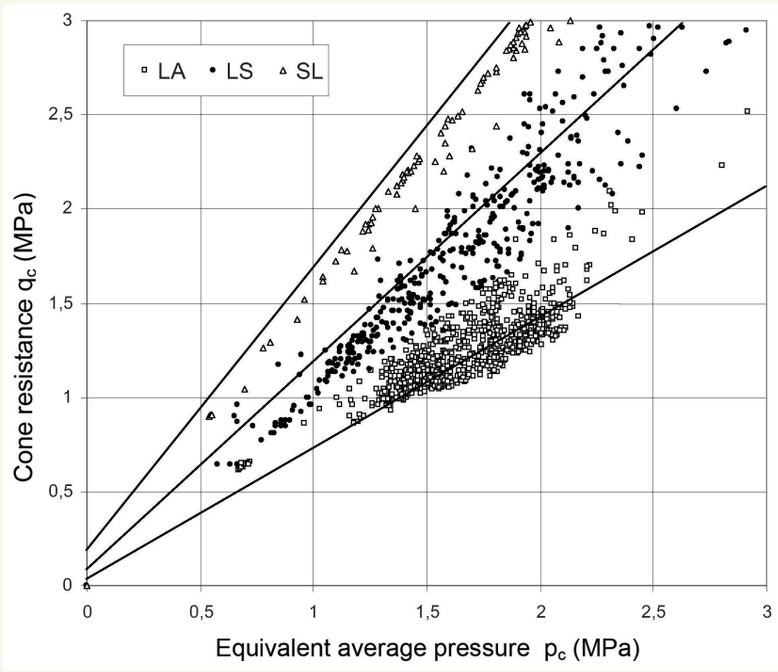

Vigure 18
Close-up of Figure 17

It must therefore be assumed, though verification proves impossible, that the water pressure u_2 has been correctly measured by the piezocone despite the absence of conditions typically implemented on the triaxial device, whose application requires the use of back pressure. It must also be assumed that this pressure directly reflects "average" pore pressure in the soil adjacent to the cone.

› The problem of loose sands

For loose silty sands, the "undrained" line runs near the line for clayey silts with low-strength characteristics. The clayey silts and loose undrained silty sands can thus be confused, if no means are available to directly identify the soil based on core samples.

› Cavitation in dense sands

A special case arises with dilatant sandy materials when the penetration is undrained. Soil shear caused by the cone produces negative water pressure ($u_2 < 0$). The measurement of these pressure drops however is limited to a certain fraction of atmospheric pressure due to the potential for cavitation within the pore fluid. The minimum pressure loss cannot exceed -60 to -80 kPa relative to atmospheric pressure, which is observed in practice. Therefore the dilatant nature of the soil becomes partially hidden.

So, the diagnosis of sands using the piezocone poses various problems due to the absence of a response in u_2 when sands are porous or due to a truncated response in u_2 when sands are highly dilatant and undrained.

› Lateral friction f_s on the piezocone coupling

In principle, the measurement of unit lateral friction provides information on the "tightening" nature of the soil around the shaft, in back of the cone, in connection with both soil dilatancy and the elastic reaction of the remote soil mass. This is the measurement however that creates the greatest difficulty with the largest uncertainties. The f_s measurement is especially open to criticism in terms of accuracy and repeatability.

› Soil mass heterogeneities

The previous developments pertain to homogeneous soil layers. In practice and within natural ground, the penetrometer response is disturbed at the transition from one soil layer to another of a different composition or else by the crossing of interspersed sandy beds (interbeds) whenever the

thickness of these beds matches the cone dimension scale. This issue needs to be examined further within the scope of the proposed method.

Recapitulation

In summary, the soil identification method based on penetrometer data q_c and u_2 (step 1) relies on an analogy between soil behaviour observed in triaxial tests and the soil response during cone penetration. Tip resistance q_c is broken down into an "isotropic" term and a "deviatoric" term in accordance with the triaxial, drained and undrained failure envelopes. This method offers the advantage of not introducing a measurement standardization process, as is the case in current methods, wherein tip resistance is standardized by means of total vertical and effective stresses in the soil mass (that are most often obtained based on hypotheses regarding soil unit weight and K_o conditions). Such information is contained in the penetrometer response. The other advantage stems from a direct incorporation of pressure u_2 in the clays, which exhibit an undrained behaviour during penetration.

IDENTIFICATION OF SENSITIVE SANDY SOILS

Given acceptance of the soil identification step on the basis of an analogy of triaxial and penetrometer responses, our attention now turns to sorting, from among the sands, those specimens displaying the weakest strength characteristics; under undrained conditions, these specimens may prove vulnerable to the liquefaction risk.

During this second step and given difficulties tied to:

– the drainage of clean sands, without the generation of water pressure since the sands are porous;
– cavitation that conceals the actual response of dense sands when undrained;
– a total lack of independence in the penetrometer data,

and after exclusively using q_c and u_2 to perform the soil identification (step 1), the remaining task consists of examining the potential contribution of f_s.

Effect of sand densification on piezocone measurements

The opportunity to study an individual worksite was provided at Fos-sur-Mer (Rhône River delta), where soil was treated using stone columns, in order to build a wharf. Three test areas were set up as a preliminary step. One of the soil improvement quantification methods introduced in this approach consisted of conducting piezocone tests before and after soil treatment. Results have been employed to demonstrate the effect of densifying a sand layer on piezocone measurements.

› Soils and their penetrometer properties

The soil mass consists of a fine-grained silty sand layer 7 to 10 m thick lying on a 10 to 13 m thick layer of clayey-sandy silts. These layers are underlain by Crau cobblestone, which form the substratum, whose roof is located approx. 20 to 23 m deep. The stone columns extend to the cobblestone, with an inter-axis distance of 2.5 m according to a triangular mesh pattern. The three test areas differ by their *in situ* position and the type of ballast used. Each zone comprises 21 columns and in each, four piezocone soundings were made prior to soil treatment and eight boreholes after treatment. The boreholes were drilled no more than 5 m apart; four of the post-treatment soundings were located immediately adjacent to the pre-treatment ones (less than 1 m away) and in between the installed columns.

The penetrometer responses are characteristic of soils encountered at the site. In sands, tip resistances q_c amounted to between 3 and 8 MPa before soil treatment and pressures u_2 were equal to the hydrostatic pressure (i.e. drained behaviour) or locally to slightly less than hydrostatic pressure. In silts, the resistances q_c were weak, less than 1 MPa, with friction values f_s below 0.02 MPa and pressures u_2 high and increasing with depth. Similarly, q_c and f_s measurements rose in a quasi-linear

pattern with depth. Sandy interbeds also appeared within the silts; these beds may be correlated between the soundings.

The idea developed herein consists of using the densification effect on fine-grained silty sands caused by the installation of stone columns in order to assess the evolution in the ratio of q_c to f_s subsequent to the increase in these strength characteristics.

› Soil treatment effect

The comparison of adjacent soundings is not direct, since the penetrometer measurement intervals differ before and after treatment; moreover, initial recording heights also differ. The probes introduced are likely to be different as well. However, after recalibrating recordings in the *z* direction through use of the peak resistance q_c upon crossing the sandy interbeds, it becomes possible to determine the densification effect ascribable to soil treatment by directly comparing penetrometer measurements before and after treatment.

This comparison **(Fig. 18)** reveals a distinct improvement in the silty sand characteristics, and this may be ascribed to their densification, with:

– a 100% average increase in q_c,
– a 40% average increase in f_s (f_s rises less with respect to q_c),
– the appearance of pressures u_2 less than the hydrostatic pressure.

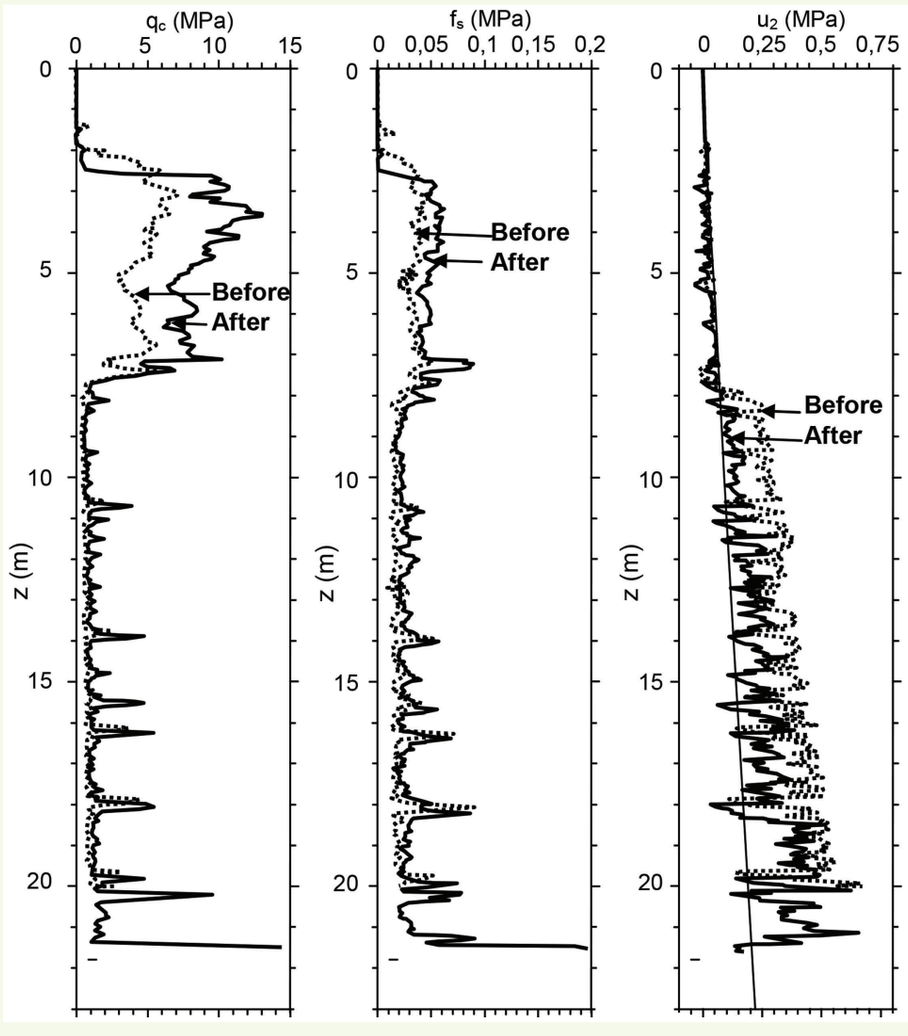

Figure 18
Comparison of 2 piezocone soundings performed before and after soil densification

Observations in the silts indicate:

– a small rise in q_c, except in the sandy beds,
– a higher f_s,
– a smaller u_2.

This reduction in u_2 may be attributed to:

– the soil densification effect due to the columns, on both the mechanical behaviour (i.e. over-consolidation) and permeability (lower void index in the sands);
– effect on drainage conditions triggered by the presence of these columns, with such an effect being promoted by the anisotropy of soil permeability;
– an eventual effect of hydraulic fracturing (soil breakdown due to column production, specifically near the surface or in the silts, which are relatively impermeable).

This treatment procedure may also cause the soil to become destructured due to the strong vibrational energy transmitted into the soils during column installation, thereby reducing the strength gain obtained through densification.

› Comparison before and after treatment in the (f_s, q_E) plane

The data provided by piezocones before and after treatment are reported using bi-logarithmic coordinates in the (f_s, q_E) plane in **Figures 19** and **20**, respectively. The variable q_E, so-called "effective" cone resistance, was introduced by Senneset *et al.* (1982). The (*lg* f_s, *lg* q_E) plane was used by Eslami and Fellenius (1997) and then Fellenius and Eslami (2000, 2004), who proposed a soil classification scheme according to data output by the piezocone. These classification results are reported in **Figure 21**.

At this site, the sands identified during step 1 are shown in green. Soil treatment has the effect of increasing both the effective cone resistance q_E, which reached 10 MPa on average, and unit lateral friction f_s. This rise takes place along a direction with slope 2 in the (*lg* f_s, *lg* q_E) plane.

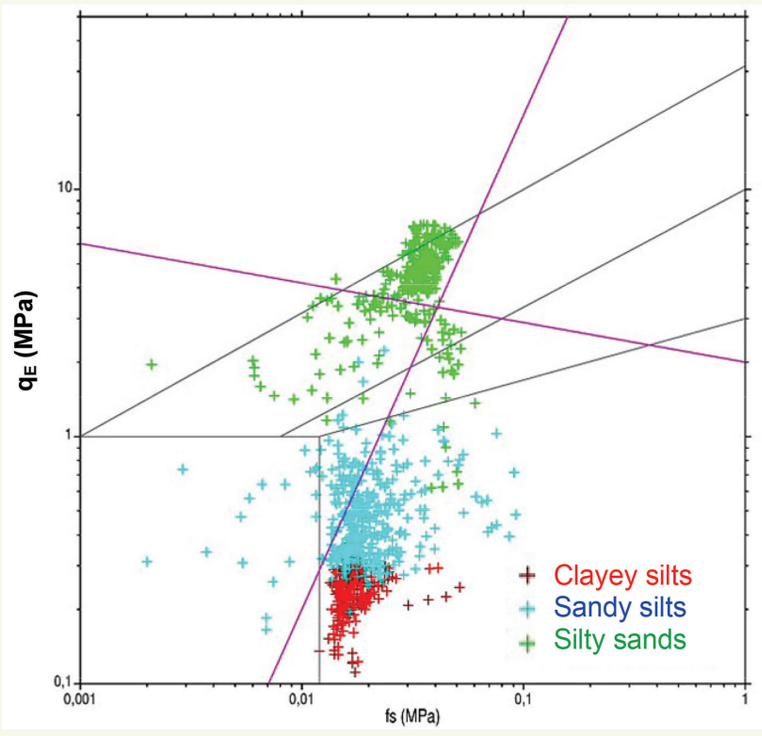

Figure 19
Representation of measurements before the soil densification (borehole 21)

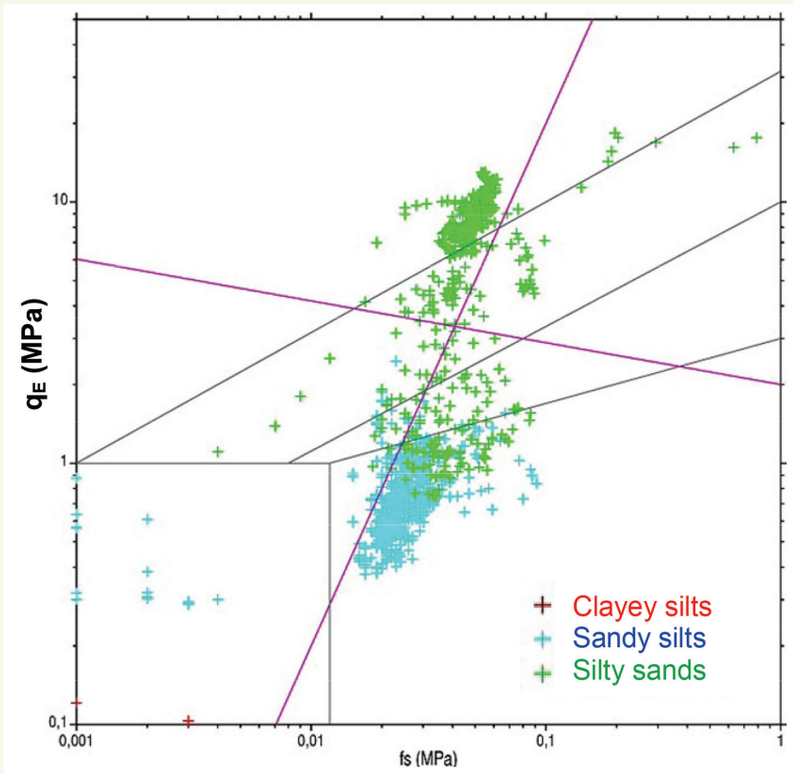

Figure 20
Representation of measurements after the soil densification (borehole 203)

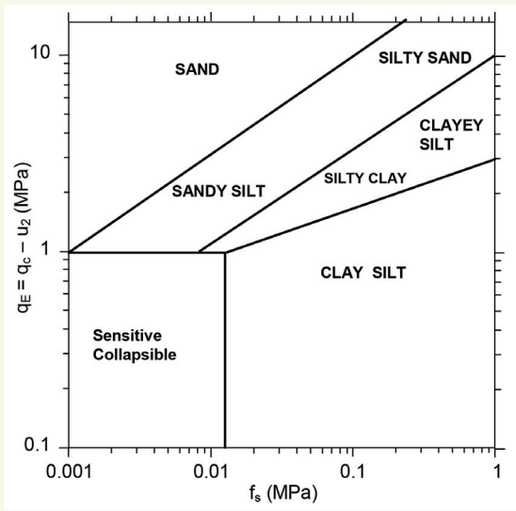

Figure 21
Soil classification according to the q_E and f_s values (Fellenius and Eslami, 2000)

Based on this example therefore, the densification of a sandy soil induces greater penetrometer strength in the direction with a slope of 2 and upwards in the ($lg\ f_s$, $lg\ q_E$) plane. In the following discussion, it will be assumed that the drop in density of a sand induces a strength decrease in the opposite direction.

Identification of sensitive sandy soils

The classification depicted in **Figure 21** does not distinguish in operational terms the loose sandy soils, which are capable of liquefaction, from the clayey or muddy soils, whose strengths are also very low and which yield data points mixed with the points for sandier soils. Though soils with sandy behaviour are distinguished during the first step of the classification process presented in this article, it is still necessary to identify which of the sandy soils are sensitive to liquefaction.

Many studies have been devoted to this important question for seismic zones and all have relied on an analysis of soils that had (or would have) liquefied during earthquakes. The words "would have" underscore a significant difficulty with this type of study, i.e. complications often involved in determining which soils have actually liquefied at a site where signs of liquefaction have been observed on the surface. Moreover, most major liquefaction accidents analysed as part of published studies have occurred within hydraulic embankments, whose state differs from that of natural soils. The transposition from one site to another and from one soil type to another in the conclusions of such studies is, for this very reason, complex and relatively unreliable. The approach presented herein has sought to circumvent this obstacle by including from the outset of the analyses the site's soil properties, as determined in laboratory tests. Nonetheless, this approach remains dependent upon the set of liquefaction observations recorded at earthquake sites, in order to identify the soil layers featuring apparently suspicious behaviour. Yet such a suspicious characterization does not imply that the soils are actually liquefiable, particularly at a site like the Var Delta plateau, where soils contain high concentrations of fine particles (which in practice prevent the development of liquefaction).

Among more recent studies, the one conducted by Ku *et al.* (2003) analysed sites where liquefaction phenomena were observed during the Chi-Chi earthquake in Taiwan. The values of f_s and q_E determined by five piezocone soundings are provided in **Figure 22**. The soils identified as sands through applying the first step of our procedure are shown by differentiating non-liquefied sands (crosses in the figure) from liquefied sands (circles), according to observations recorded by Ku *et al.* The liquefied sands are located in the lower left quadrant of the diagram and move towards non-liquefied sands along the direction with slope 2 and towards the upper part of the plane.

The sector of liquefied sands may be delimited by a line of slope 2, as well as by another line nearly orthogonal to the first with a slope of -0.16. These two lines are described by the following equations (with q_E and f_s expressed in MPa):

$$q_E = 2000\ f_s^{2},$$

$$q_E = 2\ f_s^{-0.16}.$$

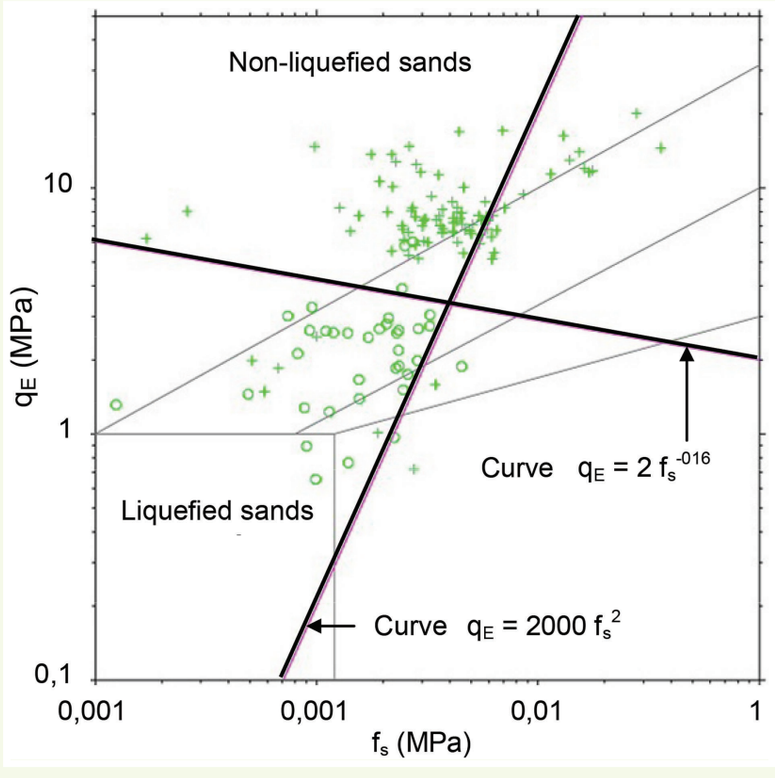

Figure 22
Analysis of the measurements conducted with the piezocone at liquefaction sites of the Chi-Chi earthquake in Taiwan (Ku et al., 2003), shown in bi-logarithmic coordinates

Figure 23 displays the same results as in **Figure 22**, yet this time using linear coordinates in the (f_s, q_E) plane. From the standpoint of the proposed method, the hyperbole (linear slope: -0.16) establishes the boundary between loose and dense sandy soils, or more precisely between non-liquefied and liquefied soils during the earthquake. The parabola (linear slope: 2) distinguishes soil types by separating this site's sandy soils from its clayey soils. The sensitive sandy soils are located adjacent to the origin point on the graph, which raises questions about the measurement accuracy of q_c, f_s and u_2. With low strengths for q_E and f_s, the soft clayey soils are also positioned near the origin of the (f_s, q_E) plane, which creates difficulties relative to the differentiation of these materials with respect to the nearby sandy soils.

Other penetrometer measurements retrieved from databases found in the literature do not strictly lie within the boundaries of the domain delimited herein. Further work is thus required for a more detailed analysis of these data and in order to assess the possibility of obtaining a general set of rules, as opposed to rules established for each site.

Recapitulation

Step 2 of the method presented in this article has consisted of identifying sensitive sandy soils. The method makes use of a measurement of unit lateral friction f_s, in acknowledging all the reserves relative to such a measurement from an experimental perspective and in acknowledging the absence of accompanying theoretical developments. According to the data input, the densification of a soil takes place along a direction of slope 2 and upwards in the ($lg\ f_s$, $lg\ q_E$) plane. It has been assumed herein that the progression towards a looser soil state occurs in the opposite direction. These considerations serve to delimit a given sector of the ($lg\ f_s$, $lg\ q_E$) plane, where sensitive sandy soils are located, but this sector also includes soft clayey soils. For this reason, soils samples have to be extracted to determine their particle size distribution and conclude on their sensitivity, according to the values of q_E and f_s.

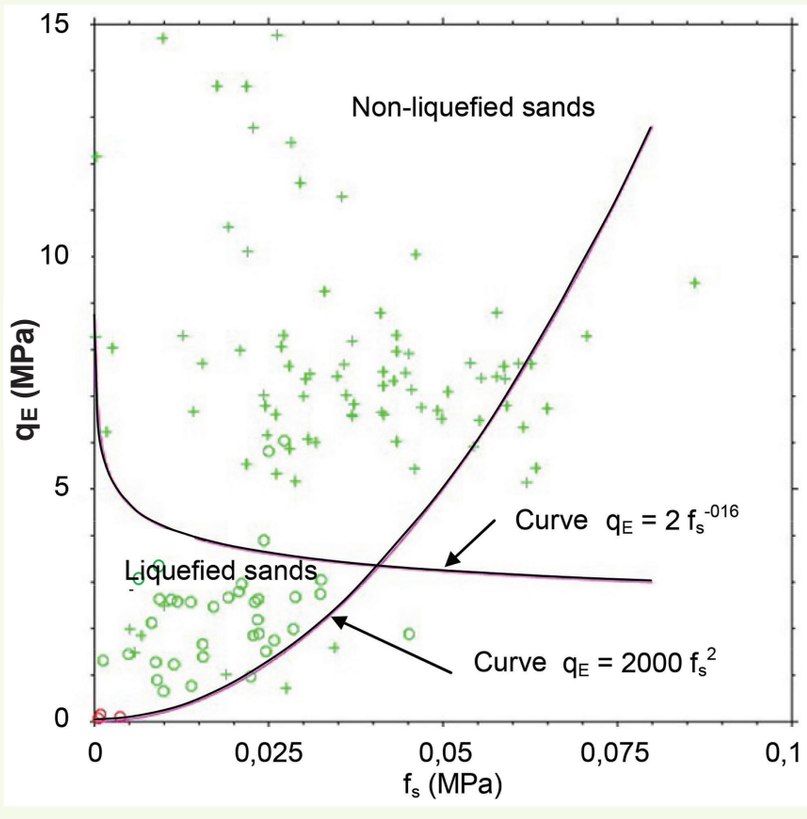

Figure 23
Analysis of the measurements conducted with the piezocone at liquefaction sites of the Chi-Chi earthquake in Taiwan (Ku et al., 2003), shown in linear coordinates

Application to Var Delta plateau soils

The most sensitive soils were identified using data from the CPTu20 sounding as a function of f_s and $q_E = q_c - u_2$, as described above.

The sets of values for both the unit lateral friction f_s and effective cone resistance q_E are first represented in linear coordinates **(Fig. 24)** and then in bi-logarithmic coordinates **(Fig. 25)**.

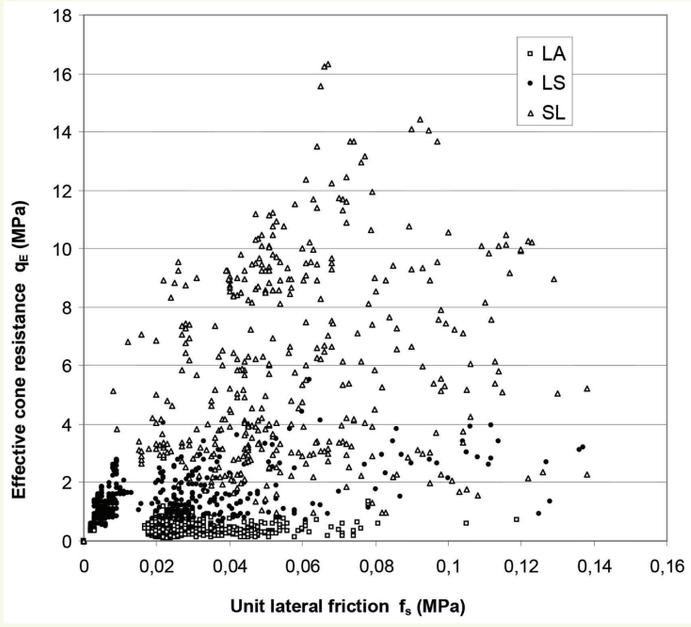

Figure 24
Representations of the CPTu20 piezocone sounding results in the "unit lateral friction f_s - effective cone resistance q_E" diagram

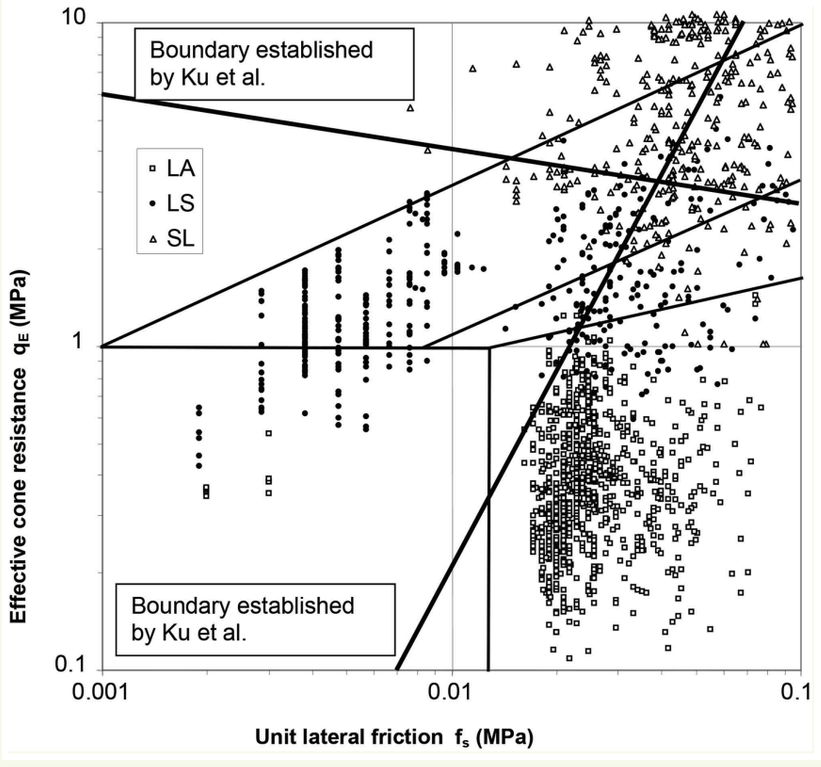

Figure 25
Extracted from Figure 24 for display using bi-logarithmic coordinates

Figure 25 also contains the lines discussed above that serve as boundaries of the Fellenius and Eslami classification system and that differentiate liquefied from non-liquefied sands, in accordance with Ku *et al.* It can be observed that a portion of the representative points for sandy silts is located in the zone of liquefied sands of the Chi-Chi earthquake. Sandy silts and clayey silts can also be assessed, yet it is assumed that these soils are not included among the sandy soils exposed to a liquefaction risk. **Figure 26** shows the positions of all points representing silty sands (as intended during the first step of the classification procedure presented herein).

The points located in the zone of liquefied sands were identified in the CPTu20 sounding. **Table 4** provides commentary on this analysis.

This analysis has shown that the presence of potentially liquefiable soils is limited. The only really thick layer should be examined in greater detail.

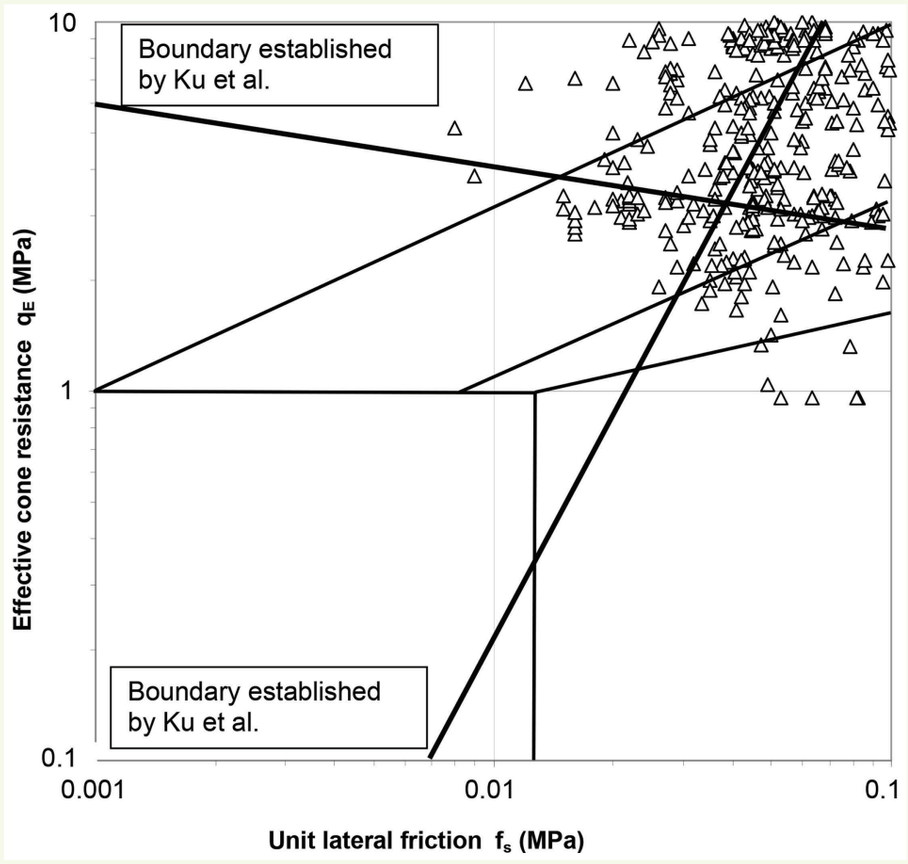

Figure 26
Analysis of the sandy soils from CPTu20 piezocone sounding

Depth (m)	Thickness (m)	Comments
14.74 - 14.78	0.06	Transition layer
15.56	0.02	Isolated point (f_s is small relative to its vicinity)
16.96 - 17.46	0.50	Part of a thicker layer in which the pore pressure is higher (yet remains less than the hydrostatic pressure). This layer should undergo a more detailed assessment, specifically by laboratory testing
20.76 - 20.78	0.06	Transition layer
23.08 - 23.10	0.06	Strong local variation
24.24	0.02	Strong local variation
Note: Measurements have been taken every 2 cm.		

Table 4
Analysis of points representing silty sands located in the zone of liquefied sands (Fig. 26)

The analysis at the scale of a piezocone sounding was repeated for all other soundings, as a contribution towards the site's overall evaluation.

CONCLUSION

A soil identification method has been proposed on the basis of data measured using the piezocone (CPTu). This method proceeds in two steps: during step 1, the tip resistance is broken down into an isotropic part and a deviatoric part, in accounting for water pressure u_2 and with reference to both the drained and undrained strength values measured beforehand on the triaxial device. This breakdown serves to classify the soils, by means of distinguishing: clayey soils, hosting the development of high water pressures; and sandy soils, whose pressures are either equal to the hydrostatic pressure or negative. Data collected at the Nice Airport site have been used to illustrate the procedure and discuss subsequent results.

Step 2 consists of identifying sensitive sandy soils, which exhibit limited compaction and low strength, especially those exposed to the liquefaction risk. The method has been based on a relative variation between f_s and q_c subjected to the densification effect for a given soil. An example was drawn from the surveying and monitoring campaign of a site strengthened by means of stone columns. The approach employed also relies on data found in the literature, offering the possibility to distinguish liquefied from non-liquefied soils during earthquakes. A sector characteristic of sensitive sandy soils was delimited in the (lgf_s, lgq_E) plane, where $q_E = q_c - u_2$ represents an "effective" tip resistance. In this manner, the three measurements derived by the piezocone are introduced into the proposed classification method.

The soil classification produced upon completion of step 1 leads to results that match the soil cross-section profiles at each of the studied sites.

Step 2 does not seem to be as relevant, given the difficulties encountered, beginning with piezocone measurement accuracy since the goal here is to search for weak soils, whether they be sandy or clayey. The available databases are sometimes contradictory. Nonetheless, the exposed sensitive soil levels in the studied penetrometer profiles match the results presented by various authors in a large majority of cases.

In summary, the proposed method conforms to methods currently in use in the area of penetrometer surveying, by including a soil identification step, followed by a step intended to identify sensitive soils. However, as opposed to methods currently applied to determine basic soil properties for project-specific needs (most often by means of empirical correlations), the proposed method seeks to benefit from triaxial tests in order to interpret the penetrometer data. It therefore assumes that the underlying geotechnical surveying calls for producing both core samples and penetrometer soundings, resulting in a dedicated analysis for the given study site. Moreover, this method does not claim to offer a universal approach, by adopting a unique soil classification protocol.

Along these lines, the rationale introduced has been inspired by the proposal made by Schmertmann (1978), who via the chart he developed was clearly not suggesting a universal soil classification nomenclature, but instead a guide for establishing such a classification dedicated to a given site or region.

The method still needed to be consolidated through wider implementation by relying on additional examples. Developments are needed for expressing undrained strength characteristics, as measured in triaxial tests, with respect to the compatibility of strain levels between triaxial and piezocone methods, and to the variability of the mechanical properties of natural soils. From this standpoint, the question extracting intact samples for laboratory study remains pertinent. The focus also lies on compiling a body of detailed examples to link with precision the properties measured in the laboratory on core samples (identification testing and triaxial tests) and piezocone measurements, not only for natural clayey and sandy soils but for intermediate silty soils as well.

Other questions still remain, like the effect of heterogeneities (interfaces between layers or sandy interbeds) or metrological and measurement accuracy aspects. It would be preferable to draw stronger correlations between the results of physical, analytical or numerical models and the proposed method. Moreover, transitions remain to be found with structural calculation methods used in project settings, such as the liquefaction risk assessment.

REFERENCES

Cetin O.K., Youd T.L., Seed R.B., Bray J.D., Stewart J.P., Durgunoglu T., Lettis W., Yilmaz M.T. (2004). Liquefaction-induced lateral spreading at Izmit Bay during the Kocaeli (Izmit)-Turkey earthquake. Journal of Geotechnical and Geoenvironmental Engineering., vol. 130, n° 12, pp. 1300-1313.

Chang M.F., Teh C.I., Cao L.F. (2001). Undrained cavity expansion in modified Cam clay: II Application to the interpretation of the piezocone test. Géotechnique, vol. 51, n° 4, pp. 335-350.

De Mio G., Giacheti H.L. (2007). The use of piezocone tests for high-resolution stratigraphy of Quaternary Sediment Sequences in the Brazilian coast. Annals of the Brazilian Academy of Sciences, vol. 79, n° 1, pp. 153-170.

Eslami A., Fellenius B.H. (1997). Pile capacity by direct CPT and CPTu methods applied to 102 case histories. Canadian Geotechnical Journal, vol. 134, n° 6, pp. 880-898.

Fellenius B.H., Eslami A. (2000). Soil profile interpreted from CPTu data. «Year 2000 Geotechnics», Geotechnical Engineering Conference, Asian Institute of Technology, Bangkok, Thailand, 27-30 novembre 2000, 18 p.

Fellenius B.H., Eslami A. (2004). CPT and CPTu data for soil profile interpretation: review of methods and proposed new approach. Iranian Journal of Science & Technlology, Transaction B, vol. 28, n° B1, pp. 69-86.

Ku C.H., Lee D.H., Juang H.C., Wu J.H. (2003). Evaluation of soil liquefaction in the Chi-Chi, Taiwan earthquake using CPT data. Soil Dynamics and Earthquake Engineering, vol. 24, n° 9-10, pp. 659-673.

Nash D.F.T., Powell J.J.M., Lloyd I.M. (1992). Initial investigations of the soft clay test site at Bothkennar. Géotechnique, n° 42, vol. 2, pp. 163-181.

Schmertmann J.H. (1978). Guidelines for cone test, performance and design. Federal Highway Administration, Report FHWA-TS-78209, Washington, 145 p.

Schneider J.A., Peuchen J., Mayne P.W., McGillivray A.V. (2001). Piezocone profiling of residual soils. Proceedings, International Conference on In Situ Measurements of Soil Properties and Case Histories, Bali, Indonesia, pp. 21-24.

Senneset K., Jambu N., Svano G. (1982). Strength and deformation from cone penetration tests. Proceedings 2nd. European Symposium on Penetration Testing, ESOPT-II, Amsterdam, vol. 2, pp. 863-870.

Simonini P., Cola S. (2000). Use of piezocone to predict maximum stiffness of Venetian soils. Journal of Geotechnical and Geoenvironmental Engineering, vol 126, n° 4, pp. 378-382.